The Astrophysical Journal, 619:639–655, 2005 January 20

IMPROVED LABORATORY TRANSITION PROBABILITIES FOR Pt I AND APPLICATION TO THE PLATINUM ABUNDANCES OF BD +17°3248 AND THE SUN

E. A. Den Hartog, M. T. Herd, and J. E. Lawler
Department of Physics, University of Wisconsin, Madison, WI 53706; eadenhar@wisc.edu, mherd@wisc.edu, jelawler@wisc.edu

C. Sneden
Department of Astronomy and McDonald Observatory, University of Texas, Austin, TX 78712; chris@verdi.as.utexas.edu

J. J. Cowan
Department of Physics and Astronomy, University of Oklahoma, Norman, OK 73019; cowan@nhn.ou.edu

and

T. C. Beers
Department of Physics and Astronomy and JINA: Joint Institute for Nuclear Astrophysics,
Michigan State University, East Lansing, MI 48824; beers@pa.msu.edu
Received 2004 June 14; accepted 2004 September 28

ABSTRACT

Radiative lifetimes, accurate to ±5%, have been measured for 58 odd-parity levels of Pt I using laser-induced fluorescence. The lifetimes were combined with branching fractions measured using grating and Fourier transform spectrometry to determine transition probabilities for 127 lines of Pt I. The new Pt lifetime measurements were found to be in good agreement with previous but less extensive measurements based on laser-induced fluorescence. The new branching fraction measurements were found to be in fair agreement with one earlier study. Absolute atomic transition probabilities from the new measurements were used to determine the platinum abundance in the metal-poor Galactic halo star BD +17°3248. An attempt to refine the solar photospheric abundance of platinum was unsuccessful; the single Pt I line used in an earlier abundance determination was found to be even more severely blended than expected from earlier work.

Subject headings: atomic data — stars: abundances — Sun: abundances

Online material: machine-readable tables

1. INTRODUCTION

High-resolution, high signal-to-noise ratio (S/N) spectra from very large ground-based telescopes and the *Hubble Space Telescope* (*HST*) are providing new insights into the roles of the *r*(rapid)- and *s*(slow)-processes in the initial burst of Galactic nucleosynthesis. Recent abundance determinations of heavy neutron-capture (*n*-capture) elements in very metal-poor stars have revealed nearly pure *r*-process abundance patterns in some of these stars (Gratton & Sneden 1994; McWilliam et al. 1995; Cowan et al. 1995; Sneden et al. 1996; Ryan et al. 1996). Heavy ($A \sim 200$) elements in the third *n*-capture peak (Os, Ir, Pt) were first detected in metal-poor star HD 126238 and more recently in HD 115444 using *HST* (Cowan et al. 1996; Sneden et al. 1998). The important lines of the elements in the third *n*-capture peak are in the ultraviolet (UV), and thus observations using the *HST* are needed for abundance determinations on these elements. The determination of accurate, absolute atomic transition probabilities for deep UV lines of these elements represents a challenge for laboratory spectroscopists, but such lab data are essential for reducing uncertainties in the inferred abundances of these elements.

The current work on Pt I is part of a continuing effort to improve the transition parameters for heavy *n*-capture elements and thereby refine the abundance determinations for those species. Improved transition probability data for numerous spectra have been published over the last few years, including La II (Lawler et al. 2001a), Ce II (Palmeri et al. 2000), Pr II (Ivarsson et al. 2001), Nd II (Den Hartog et al. 2003), Sm II (Xu et al. 2003), Eu I, II, and III (Den Hartog et al. 2002; Lawler et al. 2001c), Tb II (Den Hartog et al. 2001; Lawler et al. 2001b), Dy I and II (Curry et al. 1997; Wickliffe et al. 2000), Ho I and II (Den Hartog et al. 1999; Lawler et al. 2004), Tm I and II (Anderson et al. 1996; Wickliffe & Lawler 1997), Lu I, II, and III (Den Hartog et al. 1998; Quinet et al. 1999; Fedchak et al. 2000), Os I and Ir I (Ivarsson et al. 2003), Th II and III (Biémont et al. 2002; Nilsson et al. 2002b), and U II (Lundberg et al. 2001; Nilsson et al. 2002a). The solar abundances of several of these elements have been brought into agreement with meteoritic abundances through improvements in the transition probability database (see, e.g., Bord et al. 1998; Den Hartog et al. 1998; Lawler et al. 2001b).

The next section describes our new radiative lifetime measurements on 58 odd-parity levels of Pt I, and § 3 describes our branching fraction measurements for 127 lines. Section 4 reports astrophysical applications of these new data, including a determination of the platinum abundance in the metal-poor Galactic halo star BD +17°3248 and an attempt to refine the solar photospheric platinum abundance.

2. RADIATIVE LIFETIMES

Radiative lifetimes of 58 odd-parity levels of Pt I have been measured at the University of Wisconsin using time-resolved laser-induced fluorescence. The technique and details of the apparatus have been described in detail elsewhere, and only an abbreviated description is given here. For more detail the reader is referred to recent work in Eu I, II, and III (Den Hartog et al. 2002) and Tb II (Den Hartog et al. 2001).

A large-bore hollow cathode discharge is used as a sputter source of platinum atoms. The discharge is operated in 0.4 torr argon with 10 μs duration, 7 A peak current pulses. These pulses are superposed on a 30 mA DC current, which keeps the discharge lit. The hollow cathode is closed at one end except for a 1 mm hole, through which a slow, weakly collimated beam of platinum atoms is extracted into a low-pressure (10^{-4} torr) scattering chamber. The beam contains atoms in the ground level, as well as in metastable levels up to $\sim$20,000 cm^{-1}, which can serve as lower levels for laser excitation. The beam density and the background pressure are low enough that radiation trapping and collisional depopulation of excited levels are not observed.

The atomic beam is crossed at right angles by a laser beam 1 cm below the nozzle of the hollow cathode. The laser beam is produced by a nitrogen laser-pumped dye laser, which produces $\sim$5 ns pulses with a 0.2 cm^{-1} bandwidth. The wavelength range of this laser, including the use of frequency-doubling crystals, is from 2050 to 7200 Å. The narrow bandwidth and extensive wavelength range of the laser, as well as the flexibility in choice of lower level, allows for the selective excitation of energy levels up to $\sim$57,000 cm^{-1}. Fluorescence from the excited level is collected in a direction mutually orthogonal to the two beams using a pair of fused-silica lenses that make up an f/1 optical system. The fluorescence is detected with a 1P28A photomultiplier tube (PMT), and a decay curve, consisting of an average over 640 individual pulses, is recorded with a Tektronix SCD1000 digitizer. The laser wavelength is then tuned off the excitation transition, and a background trace is recorded. A linear least-squares fit to a single exponential is performed on the background-subtracted decay to yield the lifetime of the excited level. The lifetime of each level is measured five times during ''run one'' and is later remeasured five times during ''run two'' using a different laser transition whenever possible. This duplication helps to ensure that the transitions are identified correctly, are free from blends, and are correctly classified.

Lifetimes of neutral atoms from 2 ns up to $\sim$3 μs can be measured with this apparatus. The lower limit is determined by the bandwidth of the electronics. The upper limit arises from the atoms in the beam leaving the viewing region before they fluoresce, causing an apparent shortening of the level lifetime. This time-of-flight effect is mitigated for longer lifetimes (>300 ns) by inserting a third lens in the optical collection system, so as to effectively defocus the fluorescence at the PMT. This lens makes the system much less sensitive to the motion of the atoms, but at a cost of a factor of 4–5 in S/N.

Several other systematic effects must be controlled to avoid distortion of the exponential fluorescence decay. Unwanted fluorescence from cascades or blends can sometimes be eliminated with the use of an optical filter inserted between the two collection lenses. In Pt I, cascade fluorescence from lower lying levels is not much of a problem because of a nearly complete lack of overlap of the odd and even configurations within the range of energy levels studied. Cascade contributions from higher levels are not an issue in this experiment because of the selective nature of the excitation. Another potential source of distortion is from Zeeman quantum beats. These beats occur when the polarized laser produces dipole-aligned atoms, which then precess in the Earth's magnetic field. The anisotropic radiation pattern rotating through the viewing direction produces an oscillation of the observed fluorescence. This effect can be controlled by maintaining a near-zero ($\pm$20 mG) field in the scattering chamber with Helmholtz-like coils. For lifetimes greater than 300 ns, the necessary tolerance on the field becomes difficult to achieve. In this case a high field (30 G) is maintained, resulting in very rapid oscillations that average to zero on the timescale of the lifetime.

The Pt I lifetimes reported here, with the exception of lifetimes under 4 ns, have uncertainties of $\pm$5%. To maintain this level of uncertainty over a wide dynamic range, we periodically perform end-to-end tests of the experiment by comparing our measurements of certain lifetimes, or ratios of lifetimes, of other elements with the well-known values for these lifetimes or ratios. These cross-checks are discussed in detail in Den Hartog et al. (2002). They include lifetimes for levels in Be I (Weiss 1995), Be II (Yan et al. 1998), and Fe II (Guo et al. 1992; Biémont et al. 1991), covering the range from 1.8 to 8.8 ns. He I lifetimes are measured in the range 95–220 ns (Kono & Hattori 1984). In addition, relative absorption oscillator strengths of Fe I (Blackwell et al. 1979a, 1979b) are used to calculate accurate ratios of lifetimes that tie together lifetimes near 6, 60, and 90 ns. These ratios help fill in the gap between 30 and 95 ns where there are no convenient benchmark lifetimes to measure. We have recently added a new cross-check near 30 ns. This is the lifetime of the $4p'[1/2]_1$ level of Ar I, measured to be 27.85(7) ns by Volz & Schmoranzer (1998) using beam-gas laser spectroscopy. By measuring these cross-checks periodically, we verify that the experiment is producing reliable and consistent results.

Our results of lifetime measurements of 58 odd-parity levels of Pt I are presented in Table 1. Energy levels are taken from Blaise et al. (1992a), and the air wavelengths are computed from the energy levels using the standard index of air (Edlén 1953, 1966). The uncertainty of the lifetimes is $\pm$5%, with the exception of lifetimes shorter than 4 ns, in which case the uncertainty is $\pm$0.2 ns.

A comparison of our results and lifetimes available in the literature appears in Table 2. Our results are in good agreement with the earlier LIF measurements of Gough et al. (1982). All of our results agree within the combined uncertainties. The mean difference between our measurements and theirs is $-$1.4%, and the rms difference is 3.2%. This level of agreement between independent LIF measurements is now routine. The agreement is not so good with the beam-sputtering measurements of Ramanujam & Andersen (1978). We are in reasonable agreement with the two short-lived levels at 32,620 and 34,122 cm^{-1} but see a marked discordance with the two longer lived levels. The mean and rms differences between our measurements and theirs are +11.5% and 23.9%, respectively.

3. BRANCHING FRACTIONS AND ATOMIC TRANSITION PROBABILITIES

Branching ratios from grating spectrometer measurements in our University of Wisconsin (UW) lab were combined with branching ratios from spectra recorded with the 1 m Fourier transform spectrometer (FTS) of the US National Solar Observatory (NSO) to determine complete sets of branching fractions for Pt I levels. Figure 1 is a block diagram that shows the energy of the Pt I configurations included in this study. The FTS spectra from the NSO on Kitt Peak, AZ, provided excellent coverage at lower wavenumbers (<40,000 cm^{-1}), but the performance of the FTS at higher wavenumbers was not adequate for this study. Although the 1 m FTS has been used to record spectra to 50,000 cm^{-1}, the low sensitivity of the FTS in the deep UV makes it difficult to achieve good S/Ns in neutral atom spectra from a hollow cathode lamp operating at a sufficiently low current to eliminate the need for optical depth

TABLE 1

LIFETIMES OF ODD-PARITY LEVELS IN Pt I

Energy[a] (cm^{-1})	J	Leading Component[a]	Laser Wavelength in Air[b] (Å)	Lifetime[c] (ns)
30156.854	4	$5d^8 6s 6p(^4F)^5D$	3315.04, 3408.13	643
32620.018	2	$5d^9 6p\ ^3P$	3064.71, 3139.39	13.8
33680.402	5	$5d^8 6s 6p(^4F)^5F$	3042.63	130
34122.165	3	$5d^9 6p\ ^3F$	2929.79, 2997.96	16.9
35321.653	3	$5d^8 6s 6p(^4F)^5D$	2830.29, 2893.86	27.4
36296.310	4	$5d^8 6s 6p(^4F)^5G$	2818.25, 3818.69	1006
36844.710	1	$5d^9 6p\ ^3P$	2771.66, 3255.91	18.2
37342.101	2	$5d^9 6p\ ^3P$	2677.15, 2733.96	11.7
37590.569	4	$5d^9 6p\ ^3F$	2659.45, 2719.03	8.5
37769.073	3	$5d^9 6p\ ^3D$	2646.88, 2702.40	7.2
38536.160	5	$5d^8 6s 6p(^4F)^5F$	2650.85	104
38815.908	2	$5d^8 6s 6p(^2D)^3F$	2628.03, 3100.03	13.3
40194.228	4	$5d^8 6s 6p(^4F)^5F$	2487.17, 2539.21	35.4
40516.243	2	$5d^8 6s 6p(^4F)^5D$	2467.40, 2515.58	27.9
40787.857	2	$5d^8 6s 6p(^4P)^5P$	2498.50, 2921.38	55.8
40873.529	0	$5d^8 6s 6p(^2D)^3P$	3251.98	68.0
40970.165	3	$5d^8 6s 6p(^4F)^5G$	2440.06, 2487.17, 2905.90	20.4
41802.744	1	$5d^8 6s 6p(^2D)^3D$	2436.69, 3156.56	21.5
42660.058	3	$5d^8 6s 6p(^4F)^5D$	2389.54, 3071.93	115
43187.836	1	$5d^8 6s 6p(^4F)^5D$	2357.11, 2698.43	8.0
43945.543	3	$5d^8 6s 6p(^4P)^5P$	2318.30, 2674.57	62.8
44432.663	4	$5d^8 6s 6p(^4F)^5G$	2249.90, 2292.40	47.5
44444.364	2	$5d^8 6s 6p(^4F)^5F$	2249.31, 2913.54	15.2
44730.313	3	$5d^8 6s 6p(^2F)^3$D	2274.38, 3200.71	16.7
45398.478	1	$5d^8 6s 6p(^4P)^5P$	2834.71, 3343.90	72.9
46170.386	2	$5d^9 6p\ ^3F$	2202.22, 2524.31	11.5
46419.962	2	$5d^8 6s 6p(^4P)^5D$	2508.50, 2754.91	10.4
46433.912	0	$5d^8 6s 6p(^4P)^5D$	2753.85	21.0
46622.489	3	$5d^8 6s 6p(^2F)^3D$	2180.50, 2495.81	7.6
46792.965	5	$5d^8 6s 6p(^4F)^3G$	2174.68	5.2
46963.670	4	$5d^8 6s 6p(^4P)^5D$	2166.64, 2713.13	10.5
47740.565	1	$5d^9 6p\ ^1P$	2403.09, 3100.96	4.6
48351.94	4	$5d^8 6s 6p(^4F)^3F$	2067.51, 2103.34	6.2
48535.596	2	$5d^8 6s 6p(^4F)^5G$	2059.68, 2603.14	37.0
48779.337	3	$5d^8 6s 6p(^4F)^3D$	2084.60, 2368.28	2.8
49286.116	3	$5d^8 6s 6p(^4P)^5P$	2062.79, 2340.18	8.3
49544.565	1	$5d^9 6p\ ^3D$	2303.21, 2536.49	8.0
49880.883	2	$5d^9 6p\ ^3D$	2308.04, 2515.03	5.9
50010.155	4	$5d^8 6s 6p(^2F)^3F$	2505.92	11.4
50055.313	1	$5d^8 6s 6p(^4F)^5F$	2276.42, 2298.78, 2893.22	19.1
50387.66	0	$5d^9 6p\ ^3P$	2483.37, 3141.66	18.4
51097.529	3	$5d^8 6s 6p(^4P)^5D$	2244.98, 2658.69	10.8
51286.946	2	$5d^8 6s 6p(^2F)^1D$	2428.20, 2429.10, 2645.37	6.0
51545.544	3	$5d^8 6s 6p(^4F)^3D$	2222.61	2.8
51753.317	2	$5d^8 6s 6p(^2F)^3F$	2401.00, 2401.88	22.7
52071.684	1	$5d^8 6s 6p(^4P)^5D$	2383.64, 2733.68	9.7
52520.13	4	$5d^8 6s 6p(^2F)^3F$	2357.58	5.3
52708.365	2	$5d^8 6s 6p(^4P)^5D$	2347.16, 2928.10	24.4
53019.303	1	$5d^8 6s 6p(^2F)^3D$	2152.09, 2330.97	10.6
53665.25	1	$5d^8 6s 6p(^2P)^3D$	2122.57, 2488.73	15.7
53953.379	2	$5d^8 6s 6p(^2P)^3P$	2109.66, 2280.49	7.5
54011.150	3	$5d^8 6s 6p(^4P)^5P$	2596.00, 3119.80	15.1
54178.47	4	$5d^8 6s 6p(^4P)^5D$	2268.84	8.3
54839.206	3	$5d^8 6s 6p(^4P)^3D$	2070.94, 2418.06, 2541.35	4.6
55216.828	1	$5d^9 6p\ ^3D$	2217.35, 2396.17	5.2
55536.276	3	$5d^8 6s 6p(^2P)^3D$	2201.01, 2377.96	12.2
56670.20	2	$5d^8 6s 6p(^4P)^3P$	2147.39, 2315.50	2.45
57041.73	1	$5d^8 6s 6p(^4P)^3P$	2295.74	2.55

[a] Energy levels and leading components are from Blaise et al. (1992a).

[b] Air wavelengths are computed from the energy levels using the standard index of air (Edlén 1953, 1966).

[c] The lifetime uncertainties are the larger of ±5% or ±0.2 ns.

TABLE 2
COMPARISON OF LIFETIMES OF ODD-PARITY LEVELS IN Pt I

Energy[a] (cm^{-1})	J	Lifetime (ns)		
			Other Experiments	
		This Experiment	LIF[b]	Non-LIF[c]
30156.854	4	643 ± 32	680 ± 30	400 ± 40
32620.018	2	13.8 ± 0.7	14.0 ± 0.3	16 ± 2
33680.402	5	130 ± 6	130 ± 3	98 ± 10
34122.165	3	16.9 ± 0.8	17.2 ± 0.5	17 ± 2
35321.653	3	27.4 ± 1.4	26.7 ± 0.7	...
36296.310	4	1006 ± 50	1010 ± 50	...
36844.710	1	18.2 ± 0.9	18.2 ± 0.5	...
37342.101	2	11.7 ± 0.6	11.7 ± 0.3	...
37590.569	4	8.5 ± 0.4	8.7 ± 0.5	...
37769.073	3	7.2 ± 0.4	7.7 ± 0.3	...
38536.160	5	104 ± 5	104 ± 3	...
38815.908	2	13.3 ± 0.7	13.1 ± 0.3	...
43187.836	1	8.0 ± 0.4	8.5 ± 0.6	...
44444.363	2	15.2 ± 0.8	14.8 ± 0.5	...
46419.962	2	10.4 ± 0.5	10.7 ± 0.5	...

[a] Energy levels are from Blaise et al. (1992a).
[b] Gough et al. (1982).
[c] Ramanujam & Andersen (1978).

corrections. The next subsection describes the UW grating spectrometer measurements, and the subsequent subsection describes the FTS measurements. Absolute atomic transition probabilities, determined by combining our branching fraction measurements with radiative lifetimes from the preceding section, are presented. The final subsection includes comparisons of our branching fractions and branching ratios with earlier measurements.

3.1. *Grating Spectrometer Measurements*

An Acton Research Corp. 1 m focal length spectrometer with a 3600 g mm^{-1} grating and a Princeton Instruments 1024 pixel thermoelectrically cooled photodiode array detector was used to determine the branching ratios of deep UV lines of Pt I. The system has a limit of resolution as small as 0.32 cm^{-1}, and it provides spectral coverage of the 25,000–50,000 cm^{-1} region. The spectral coverage of this grating instrument overlaps the spectral coverage of the NSO FTS. The grating spectrometer enabled us to measure Pt I branching ratios for lines in the 40,000–50,000 cm^{-1} region where the FTS was not sufficiently sensitive. The NIST Pt-Ne Atlas (Sansonetti et al. 1992) was used to help identify lines during grating spectrometer measurements.

The emission source for the grating spectrometer measurements of Pt lines was a commercially manufactured, sealed hollow cathode discharge lamp with a fused silica window containing a neon fill. The lamp was operated between 5 and 7.9 mA; the manufacturer's suggested maximum current is 8 mA. Each line measurement was repeated 3 or more times at different current values to check for a nonnegligible optical depth. Optical depth corrections were not needed with this source. Data taken from the 1 m grating spectrometer have shown minimal drift.

In the first version of the grating spectrometer experiment, hereafter referred to as the "single spectrometer setup," light from the hollow cathode lamp was focused using a concave mirror directly onto the entrance slit of the 1 m spectrometer as shown in Figure 2*a*. Although the single spectrometer setup was quite suitable for line ratio measurements, it was found to suffer from excessive scattered light when attempts were made

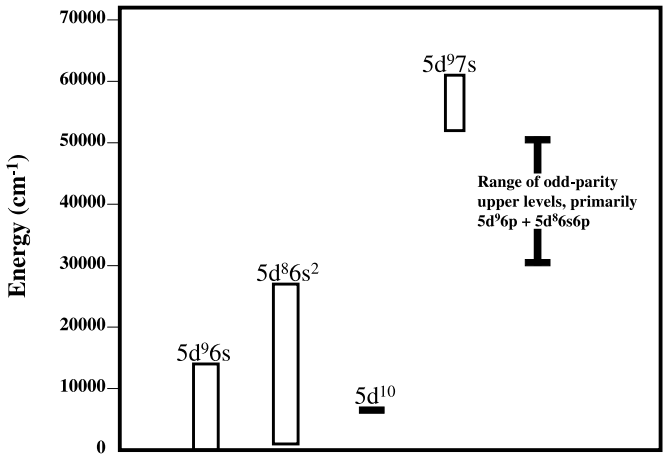

FIG. 1.—Block diagram of the Pt I configurations under study in this work.

to radiometrically calibrate the system using continuum lamps. Scattered light is one of the many difficulties in deep UV radiometric calibrations, along with optical component degradation, intrinsic uncertainties in deep UV standard lamps, and other effects. We were able to substantially reduce scattered light in the 1 m spectrometer by introducing a pre-monochromator. This 10 cm focal length monochromator was placed directly in front of the main 1 m spectrometer, such that the entrance slit of the 1 m spectrometer served as the exit slit of the 10 cm monochromator as shown in Figure 2*b*. This "double spectrometer setup" was laser aligned, but some loss of signal was inevitable from the introduction of the pre-monochromator. The concave mirror was used to focus the light from the hollow cathode lamp onto the entrance slit of the pre-monochromator. Data from both setups were used to determine branching ratios of lines with small wavenumber separations. However, data taken with the pre-monochromator were used exclusively for widely separated lines.

Two spectroradiometric calibrations were performed. One was based on an Ar miniarc lamp, and the second based on a D_2 lamp. The Ar miniarc calibration covered the 29,850–50,000 cm^{-1} region. Our primary standard in the deep UV was an Ar miniarc lamp calibrated directly by M. Bridges at NIST (see Bridges & Ott 1977; Klose et al. 1988 for discussions of the Ar miniarc as a deep UV radiometric standard). A second Ar miniarc, which served as a working standard, was used for routine tests of calibration stability.

The D_2 lamp calibration covered a larger range from 25,000 to 50,000 cm^{-1}. The UV calibrations of the 1 m spectrometer without the pre-monochromator using the Ar miniarc and D_2 lamp were in poor agreement. This discordance was due primarily to scattered light. The introduction of the pre-monochromator brought the two calibrations into satisfactory agreement. We used the Ar miniarc as our primary calibration standard and used the D_2 lamp only for a few lines at lower wavenumbers. The Ar miniarc was used without a window; thus, its calibration should be more reliable than the D_2 lamp, which has a window. Window degradation from color center formation and other effects is often a problem in spectroradiometric calibrations in the deep UV. Calibrations were performed on both the single spectrometer and double spectrometer setups including the concave mirror. Since our Ar miniarc and D_2 lamps were calibrated as spectral irradiance [power/(area × spectral interval) at a specified distance] standards, these lamps were not focused on the entrance slits of the spectrometers. Light from

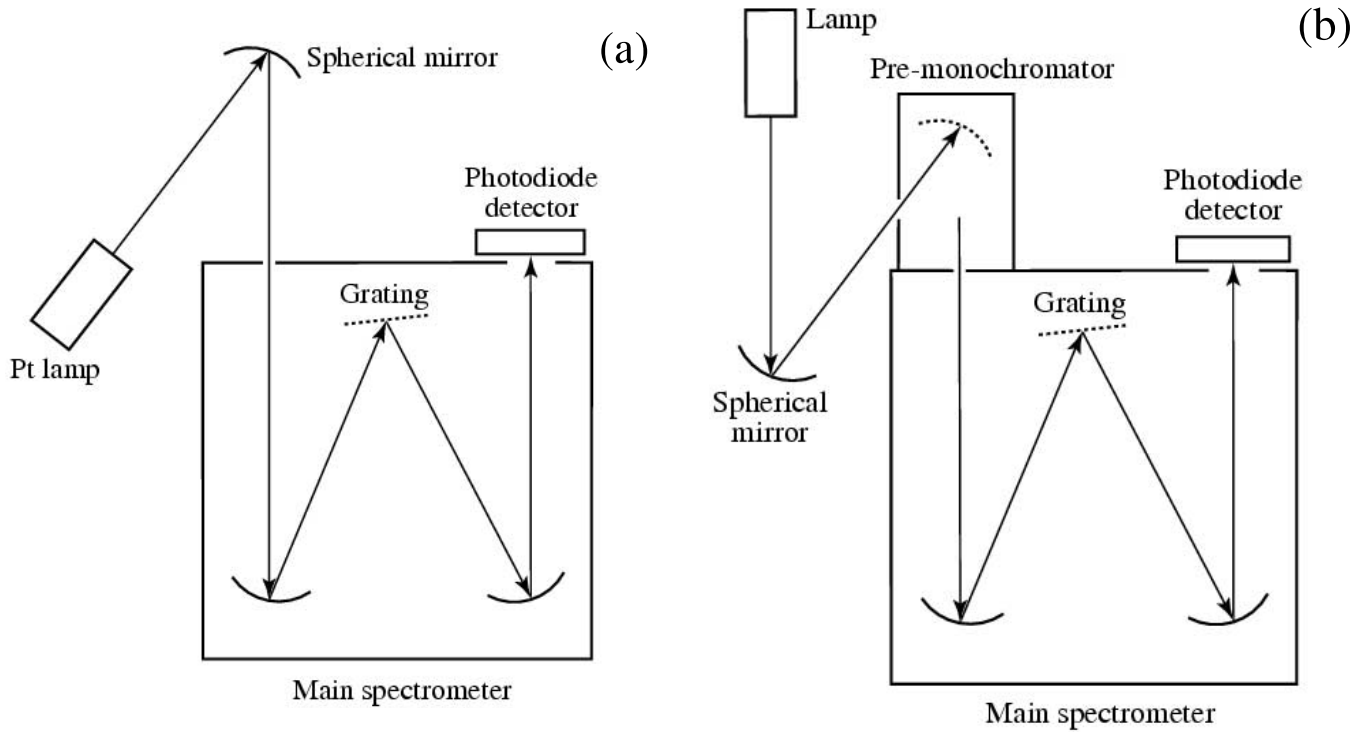

FIG. 2*a* FIG. 2*b*

FIG. 2.—(*a*) Schematic diagram of the single spectrometer setup. (*b*) Schematic diagram of the double spectrometer setup.

the standard lamps was reflected from the concave mirror and into the spectrometers, but distances were adjusted to ensure that the standard lamps' arcs were not focused on the entrance slits. The Ar miniarcs are routinely calibrated as spectral radiance [power/(area × solid angle × spectral interval)] standards. Because of the small size of the miniarc, image quality and alignment are critical when it is used as a radiance standard.

Our miniarc calibration, when used as a spectral irradiance standard, did not fill the spectrometer to the same extent as the Pt hollow cathode lamp. Possible errors introduced by differences in the filling of the spectrometer between the standard lamp and the Pt hollow cathode lamp were explored by mapping the spectrometer response as a function of wavenumber for a range of input angles. Variations in the wavenumber dependence of the radiometric calibration were not significant.

3.2. *Fourier Transform Spectrometer Measurements and Absolute Transition Probabilities*

Branching ratios for lines in the UV below 40,000 cm^{-1} and in the visible were measured on the FTS spectra. The NSO 1 m FTS is a uniquely powerful instrument that provides (1) a limit of resolution as small as 0.01 cm^{-1}, (2) wavenumber accuracy to 1 part in 10^8, (3) broad spectral coverage from the UV to IR, and (4) the capability of recording a 10^6 point spectrum in 10 minutes (Brault 1976). It also has an intrinsic advantage for branching ratio measurements. An interferogram is a simultaneous measurement across an entire spectrum, which makes the FTS much less sensitive to source drifts than sequentially scanned instruments. Although the FTS performance is limited in the deep UV, its performance in this region is best just after its optics have been recoated.

We did not attempt to record new Pt spectra because the recoating of the FTS optics is infrequent. Instead, we made a search of all spectra in the public digital archives of the NSO.[1] We located five Pt spectra in the NSO archives, two of which were quite useful. The first and most useful FTS spectrum in this study was No. 001 from 1983 July 25, recorded on a custom, water-cooled Pt-Ar hollow cathode lamp operating at 200 mA and 394 V with 2.5 torr of Ar. This spectrum has six co-adds, and it extends from 7614 to 49,880 cm^{-1} with a limit of resolution of 0.096 cm^{-1}. The FTS was configured with the UV beam splitter, midrange Si diode detectors, and no additional filters. Spectrum 002 from the same date, recorded under identical lamp conditions, was also useful. This spectrum has eight co-adds, and it extends from 18,929 to 37,638 cm^{-1} with a limit of resolution of 0.022 cm^{-1}. The FTS was configured with the UV beam splitter, midrange Si diode detectors, and $CuSO_4$ filters. The remaining three spectra were recorded on 1985 July 23. Spectrum 015 from this date was recorded on a high-pressure source, judging from the continuum present in the spectrum. The header file specifies that the source was operated with 1000 ppm Pt. This was most probably an inductively coupled plasma source. This spectrum has three co-adds, and it extends from 14,886 to 36,998 cm^{-1} with a limit of resolution of 0.071 cm^{-1}. The FTS was configured with the UV beam splitter, midrange Si diode detectors, and $CuSO_4$ filters. Spectrum 017 from this date was recorded on a Pt-Ne hollow cathode lamp operating at 20 mA. This spectrum has 12 co-adds, and it extends from 27,774 to 41,661 cm^{-1} with a limit of resolution of 0.020 cm^{-1}. The FTS was configured with the UV beam splitter, midrange Si diode detectors, and Solar Blind filters. Spectrum 021 from this date was also recorded on a Pt-Ne hollow cathode lamp. This spectrum has 10 co-adds, and it extends from 15,161 to 30,322 cm^{-1} with a

[1] Available at http://diglib.nso.edu/.

limit of resolution of 0.020 cm^{-1}. The FTS was configured with the UV beam splitter, midrange Si diode detectors, and $CuSO_4$ + WG345 filters.

We used the now-standard technique, based on overlapping sets of Ar I and Ar II branching ratios, to establish a relative radiometric calibration for the Pt-Ar hollow cathode spectra from 1983 July 25. Sets of Ar I and Ar II lines have been established for this purpose in the range of 4300–35000 cm^{-1} by Whaling et al. (1993), Hashiguchi & Hasikuni (1985), Danzmann & Kock (1982), and Adams & Whaling (1981). These provided an excellent means of calibrating our FTS spectra, since the argon lines are measured in the exact experimental arrangement and at the exact same time as are the Pt I lines. The two spectra from 1983 July were the most useful for Pt branching ratio measurements, although the other higher resolution spectra were also useful for measurements on lines with small separation and in checking for blends. Strong lines to low-lying levels of Pt have large optical depths in the 1983 July spectra because the hollow cathode lamps were operated at 200 mA current. Weak lines to higher lying levels of Pt had good S/Ns in the 1983 July spectra; thus, these spectra complemented our grating spectrometer measurements to yield complete sets of branching fractions for Pt upper levels.

All possible transition wavenumbers between known energy levels of Pt I (Blaise et al. 1992a, 1992b) satisfying both the parity change and ΔJ selection rules were computed and used during the analysis of FTS data. Upper levels, primarily from the $5d^9 6p$ and $5d^8 6s 6p$ configurations, ranging in energy from 30,157 to 50,388 cm^{-1}, were included. Branches to unknown levels and/or branches outside the observed spectral region can contribute errors to branching fraction measurements. Such errors are not a problem in our work on Pt I because of the favorable energy level structure of Pt I and because our best FTS spectrum covered the near-infrared down to 7600 cm^{-1}. The three lowest even-parity configurations of Pt I are the $5d^9 6s$, $5d^{10}$, and $5d^8 6s^2$, as shown in Figure 1. These three configurations have 14 levels, 13 of which are known. The missing $5d^8 6s^2\ {}^1S_0$ level is quite high in energy. This unknown level may connect to $J = 1$ odd-parity levels in this study, but such branches, if possible, are too far in the infrared to contribute a significant branching fraction error. The absence of other even-parity Pt I levels between 27,000 and 52,000 cm^{-1}, where the $5d^9 7s$ configuration starts, greatly simplified the assessment of possible missing infrared branches. We have confidence that our branching fractions are complete to a small fraction ($\sim\frac{1}{5}$ or less) of our final transition probability uncertainties (5% or more).

The same software was used to integrate the Ar calibration lines and the Pt I lines. A radiometric calibration curve was established using overlapping sets of Ar branching ratios. Branching ratios from the FTS spectra and from 1 m grating spectrometer measurements were combined to form complete sets of branching fractions for 30 levels of Pt I. The branching fractions for lines from these 30 levels were then combined with radiative lifetimes from the preceding section to determine absolute atomic transition probabilities for 127 lines of Pt I in Table 3. Weak lines with poor S/Ns were dropped from Table 3, but their effect in reducing other branches was preserved.

The procedure for determining branching fraction uncertainties was described in detail by Wickliffe et al. (2000). Branching fractions from a given upper level are defined to sum to unity. Therefore, a dominant line from an upper level has small branching fraction uncertainty by definition. Weaker lines near the dominant lines(s) tend to have uncertainties in their branching fractions limited by their S/Ns. Systematic uncertainty in the radiometric calibration is typically the most serious source of uncertainty for widely separated lines from a common upper level. Transition probability uncertainties in Table 3 were determined by combining in quadrature the branching fraction uncertainties with the ±5% uncertainty of the radiative lifetimes.

3.3. *Comparison with Earlier Measurements*

Lotrian & Guern (1982) reported complete sets of branching ratios, or branching fractions for nine levels of neutral Pt. Branching fractions from five of their nine levels overlap with our measurements; these are compared in Table 4. Lotrian & Guern used two grating monochromators in scanning mode with photoelectric detectors during their research: a 1 m instrument in the deep UV from 32,300 to 50,000 cm^{-1} and a 3.4 m instrument from 12,500 to 40,000 cm^{-1}. They operated with a limit of resolution in wavelength units of 0.3–1.0 Å. This could be as coarse as 25 cm^{-1} in the deep UV or as fine as 0.5 cm^{-1} in the near-infrared. Lotrian & Guern used a tungsten ribbon lamp for radiometric calibration at low wavenumbers and a D_2 lamp at high wavenumbers. They were careful to avoid errors from a nonnegligible optical depth. They reported uncertainties of about 10% for most lines but as large as 25% for the weakest branches. Our results are in agreement with the measurements of Lotrian & Guern for all 12 lines from the upper levels at 30,156.85, 44,444.36, and 46,170.39 cm^{-1}. Our results agree with their measurements within combined uncertainties for three of the five lines from the upper level at 32,620.02 cm^{-1}. Our branching fractions are smaller than theirs for the two lines where we disagree. There is similar discordance in the branching fractions for lines from the upper level at 34,122.16 cm^{-1}, but most of the differences in this case are due to the line 33,298.49 cm^{-1} (3002 Å air). This line is within 48 cm^{-1} of the dominant branch at 33,346.27 cm^{-1} (2998 Å) from this upper level. Indeed, the small spacing of all three of the strong lines from this upper level at 34,122.16 cm^{-1} means that radiometric uncertainty cannot be used to explain the discordance. The most likely explanation is a hidden blend in the result of Lotrian & Guern for the line at 33,298.49 cm^{-1}. Given the inherent difficulties of deep UV intensity measurements, we consider our results to be in satisfactory agreement with the earlier measurements by Lotrian & Guern.

Early in this effort to improve Pt I atomic transition probabilities we planned to combine radiative lifetimes described in the preceding section with branching fractions deduced from the intensities in the NIST Pt Atlas (Reader et al. 1990; Sansonetti et al. 1992).[2] This atlas was developed for Pt-Ne hollow cathode lamps used on *Hubble Space Telescope* (*HST*) spectrometers, including both the Goddard High Resolution Spectrograph and the Space Telescope Imaging Spectrograph. The Atlas is comprehensive in the sense that it covers a huge wavelength range and it includes many weak lines. The Pt-Ne lamps on *HST* are used primarily, or perhaps exclusively, as wavelength standards. The intensities in the NIST Atlas were reported as accurate to ±20%. The units of the intensities in the NIST Atlas are ambiguous in the publications, but units of photons/time were intended (C. J. Sansonetti 2003, private communication). Although an uncertainty of ±20% might seem undesirably large for branching fractions, one must remember that this uncertainty migrates to the weakest branches from an upper level because of the fact that branching fractions are

[2] Available at http://physics.nist.gov/PhysRefData/contents.html.

TABLE 3

ATOMIC TRANSITION PROBABILITIES FOR Pt I ARRANGED BY WAVELENGTH

λ in Vacuum[a] (Å)	λ in Air[b] (Å)	Upper Level[c] (cm^{-1})	Upper J	Lower Level[c] (cm^{-1})	Lower J	Transition Probability (10^6 s^{-1})	$\log_{10} gf$
2068.1693.....	2067.5090	48351.940	4	0.000	3	42.0 ± 2.7	−0.62
2104.0113.....	2103.3441	48351.940	4	823.678	4	119 ± 6	−0.15
2129.3055.....	2128.6332	46963.670	4	0.000	3	89 ± 4	−0.26
2154.2456.....	2153.5684	46419.962	2	0.000	3	12.1 ± 1.4	−1.38
2165.8905.....	2165.2109	46170.386	2	0.000	3	31.4 ± 1.7	−0.96
2167.3172.....	2166.6373	46963.670	4	823.678	4	3.50 ± 0.21	−1.65
2175.3655.....	2174.6839	46792.965	5	823.678	4	192 ± 10	0.18
2190.8651.....	2190.1803	46419.962	2	775.892	2	14.5 ± 1.5	−1.28
2202.9103.....	2202.2230	46170.386	2	775.892	2	31.0 ± 1.6	−0.95
2235.6204.....	2234.9262	44730.313	3	0.000	3	8.0 ± 0.6	−1.38
2250.0041.....	2249.3068	44444.364	2	0.000	3	12.8 ± 0.9	−1.31
2250.5966.....	2249.8992	44432.663	4	0.000	3	2.85 ± 0.20	−1.71
2275.0840.....	2274.3813	44730.313	3	775.892	2	28.8 ± 1.9	−0.81
2275.5436.....	2274.8408	43945.543	3	0.000	3	3.14 ± 0.19	−1.77
2289.9817.....	2289.2757	44444.364	2	775.892	2	15.2 ± 0.9	−1.22
2293.1054.....	2292.3988	44432.663	4	823.678	4	17.8 ± 0.9	−0.90
2319.0092.....	2318.2968	43945.543	3	823.678	4	9.0 ± 0.5	−1.29
2344.1131.....	2343.3952	42660.058	3	0.000	3	0.83 ± 0.09	−2.32
2357.8264.....	2357.1054	43187.836	1	775.892	2	72 ± 4	−0.74
2387.5371.....	2386.8095	42660.058	3	775.892	2	1.33 ± 0.09	−2.10
2390.2642.....	2389.5359	42660.058	3	823.678	4	3.54 ± 0.21	−1.67
2437.4281.....	2436.6891	41802.744	1	775.892	2	19.9 ± 1.2	−1.27
2451.7101.....	2450.9678	40787.857	2	0.000	3	2.41 ± 0.15	−1.96
2468.1459.....	2467.3999	40516.243	2	0.000	3	21.9 ± 1.1	−1.00
2484.1158.....	2483.3660	50387.660	0	10131.887	1	49.6 ± 2.5	−1.34
2499.2524.....	2498.4992	40787.857	2	775.892	2	14.2 ± 0.7	−1.18
2509.2528.....	2508.4972	46419.962	2	6567.461	2	15.0 ± 1.0	−1.15
2516.3341.....	2515.5769	40516.243	2	775.892	2	11.1 ± 0.6	−1.28
2525.0660.....	2524.3068	46170.386	2	6567.461	2	15.7 ± 1.1	−1.13
2620.3492.....	2619.5675	44730.313	3	6567.461	2	3.7 ± 0.3	−1.58
2628.8107.....	2628.0269	38815.908	2	775.892	2	59 ± 3	−0.51
2640.1314.....	2639.3449	44444.364	2	6567.461	2	14.6 ± 1.1	−1.12
2647.6689.....	2646.8807	37769.073	3	0.000	3	22.3 ± 1.1	−0.79
2651.6420.....	2650.8528	38536.160	5	823.678	4	9.6 ± 0.5	−0.95
2660.2417.....	2659.4505	37590.569	4	0.000	3	99 ± 5	−0.03
2675.3647.....	2674.5698	43945.543	3	6567.461	2	2.90 ± 0.22	−1.66
2677.9425.....	2677.1470	37342.101	2	0.000	3	11.7 ± 0.6	−1.20
2699.2261.....	2698.4255	43187.836	1	6140.180	0	31.7 ± 2.1	−0.98
2703.2009.....	2702.3993	37769.073	3	775.892	2	61 ± 3	−0.33
2706.6973.....	2705.8949	37769.073	3	823.678	4	42.2 ± 2.1	−0.49
2719.8383.....	2719.0328	37590.569	4	823.678	4	18.2 ± 1.0	−0.74
2730.7203.....	2729.9120	43187.836	1	6567.461	2	17.9 ± 1.4	−1.22
2734.7653.....	2733.9561	37342.101	2	775.892	2	72 ± 4	−0.40
2754.5756.....	2753.7616	46419.962	2	10116.729	3	1.15 ± 0.16	−2.19
2754.6673.....	2753.8532	46433.912	0	10131.887	1	42.6 ± 2.2	−1.31
2755.7262.....	2754.9119	46419.962	2	10131.887	1	34.4 ± 1.9	−0.71
2770.6513.....	2769.8334	42660.058	3	6567.461	2	0.67 ± 0.06	−2.27
2772.4779.....	2771.6595	36844.710	1	775.892	2	24.1 ± 1.5	−1.08
2773.6437.....	2772.8251	46170.386	2	10116.729	3	1.48 ± 0.26	−2.07
2774.8103.....	2773.9914	46170.386	2	10131.887	1	3.3 ± 0.4	−1.72
2804.0609.....	2803.2348	41802.744	1	6140.180	0	11.9 ± 0.9	−1.38
2819.0747.....	2818.2450	36296.310	4	823.678	4	0.337 ± 0.028	−2.44
2831.1246.....	2830.2919	35321.653	3	0.000	3	24.0 ± 1.2	−0.70
2835.5448.....	2834.7111	45398.478	1	10131.887	1	9.7 ± 0.5	−1.46
2889.0392.....	2888.1923	44730.313	3	10116.729	3	1.32 ± 0.18	−1.94
2894.7112.....	2893.8629	35321.653	3	775.892	2	7.7 ± 0.4	−1.17
2898.7209.....	2897.8716	35321.653	3	823.678	4	3.17 ± 0.19	−1.55
2913.1048.....	2912.2520	44444.364	2	10116.729	3	9.4 ± 1.0	−1.22
2914.3918.....	2913.5386	44444.364	2	10131.887	1	9.5 ± 1.0	−1.22
2922.2339.....	2921.3788	40787.857	2	6567.461	2	0.94 ± 0.12	−2.22
2930.6464.....	2929.7892	34122.165	3	0.000	3	22.3 ± 1.1	−0.70
2945.6138.....	2944.7529	40516.243	2	6567.461	2	0.41 ± 0.05	−2.57
2998.8359.....	2997.9618	34122.165	3	775.892	2	33.2 ± 1.7	−0.50
3003.1395.....	3002.2643	34122.165	3	823.678	4	1.76 ± 0.10	−1.78

TABLE 3—*Continued*

λ in Vacuum[a] (Å)	λ in Air[b] (Å)	Upper Level[c] (cm^{-1})	Upper J	Lower Level[c] (cm^{-1})	Lower J	Transition Probability (10^6 s^{-1})	$\log_{10} gf$
3037.3265.....	3036.4428	46419.962	2	13496.271	2	15.5 ± 1.0	−0.97
3043.5171.....	3042.6318	33680.402	5	823.678	4	7.7 ± 0.4	−0.93
3060.5267.....	3059.6371	46170.386	2	13496.271	2	1.66 ± 0.25	−1.93
3065.6022.....	3064.7114	32620.018	2	0.000	3	67 ± 3	−0.33
3072.8264.....	3071.9338	42660.058	3	10116.729	3	1.17 ± 0.18	−1.94
3100.9245.....	3100.0249	38815.908	2	6567.461	2	5.3 ± 0.4	−1.42
3140.2966.....	3139.3870	32620.018	2	775.892	2	3.53 ± 0.19	−1.58
3142.5687.....	3141.6586	50387.660	0	18566.558	1	4.8 ± 0.6	−2.15
3157.4769.....	3156.5630	41802.744	1	10131.887	1	12.1 ± 1.1	−1.27
3201.6349.....	3200.7099	44730.313	3	13496.271	2	14.4 ± 1.9	−0.81
3204.9626.....	3204.0367	37769.073	3	6567.461	2	10.5 ± 0.8	−0.95
3231.2169.....	3230.2843	44444.364	2	13496.271	2	3.7 ± 0.5	−1.54
3234.3496.....	3233.4163	46419.962	2	15501.845	2	3.5 ± 0.3	−1.57
3252.9167.....	3251.9787	40873.529	0	10131.887	1	14.7 ± 0.7	−1.63
3256.8484.....	3255.9094	36844.710	1	6140.180	0	5.3 ± 0.4	−1.60
3260.6703.....	3259.7303	46170.386	2	15501.845	2	1.9 ± 0.3	−1.83
3262.0074.....	3261.0670	40787.857	2	10131.887	1	0.054 ± 0.013	−3.36
3284.1508.....	3283.2048	43945.543	3	13496.271	2	0.24 ± 0.04	−2.56
3291.1673.....	3290.2196	40516.243	2	10131.887	1	1.64 ± 0.19	−1.88
3302.8100.....	3301.8593	36844.710	1	6567.461	2	25.3 ± 1.4	−0.91
3315.9958.....	3315.0417	30156.854	4	0.000	3	0.185 ± 0.011	−2.56
3344.8583.....	3343.8969	45398.478	1	15501.845	2	1.94 ± 0.17	−2.01
3367.9599.....	3366.9926	43187.836	1	13496.271	2	1.85 ± 0.27	−2.03
3409.1092.....	3408.1314	30156.854	4	823.678	4	1.37 ± 0.07	−1.67
3428.9100.....	3427.9271	42660.058	3	13496.271	2	1.02 ± 0.13	−1.90
3455.1243.....	3454.1347	44444.364	2	15501.845	2	0.39 ± 0.14	−2.46
3477.7538.....	3476.7584	35321.653	3	6567.461	2	0.123 ± 0.020	−2.80
3484.4202.....	3483.4231	38815.908	2	10116.729	3	1.46 ± 0.17	−1.88
3486.2616.....	3485.2640	38815.908	2	10131.887	1	7.9 ± 0.8	−1.14
3515.7173.....	3514.7121	43945.543	3	15501.845	2	0.60 ± 0.09	−2.11
3532.7609.....	3531.7513	41802.744	1	13496.271	2	0.117 ± 0.025	−3.18
3588.4282.....	3587.4044	46433.912	0	18566.558	1	5.0 ± 0.5	−2.01
3611.9350.....	3610.9051	43187.836	1	15501.845	2	0.48 ± 0.09	−2.55
3622.6860.....	3621.6533	46170.386	2	18566.558	1	0.41 ± 0.09	−2.40
3629.1444.....	3628.1100	34122.165	3	6567.461	2	1.06 ± 0.08	−1.84
3664.1330.....	3663.0896	40787.857	2	13496.271	2	0.27 ± 0.04	−2.56
3673.0444.....	3671.9987	37342.101	2	10116.729	3	0.91 ± 0.12	−2.04
3675.0905.....	3674.0443	37342.101	2	10131.887	1	0.57 ± 0.07	−2.24
3682.1274.....	3681.0793	42660.058	3	15501.845	2	0.091 ± 0.015	−2.89
3700.9661.....	3699.9132	40516.243	2	13496.271	2	0.54 ± 0.08	−2.26
3802.1514.....	3801.0722	41802.744	1	15501.845	2	1.80 ± 0.29	−1.93
3816.1612.....	3815.0784	43187.836	1	16983.492	0	0.43 ± 0.09	−2.55
3819.7708.....	3818.6871	36296.310	4	10116.729	3	0.66 ± 0.04	−1.89
3864.3152.....	3863.2199	44444.364	2	18566.558	1	0.31 ± 0.06	−2.46
3949.5037.....	3948.3862	38815.908	2	13496.271	2	0.82 ± 0.12	−2.02
3954.7557.....	3953.6368	40787.857	2	15501.845	2	0.029 ± 0.007	−3.47
3967.4787.....	3966.3565	35321.653	3	10116.729	3	1.40 ± 0.16	−1.64
3997.6976.....	3996.5675	40516.243	2	15501.845	2	0.24 ± 0.04	−2.54
4119.8375.....	4118.6755	37769.073	3	13496.271	2	2.9 ± 0.4	−1.29
4165.7231.....	4164.5491	34122.165	3	10116.729	3	0.61 ± 0.07	−1.95
4193.6053.....	4192.4240	37342.101	2	13496.271	2	0.72 ± 0.10	−2.02
4289.2567.....	4288.0502	38815.908	2	15501.845	2	0.22 ± 0.04	−2.52
4303.6323.....	4302.4220	41802.744	1	18566.558	1	0.52 ± 0.10	−2.36
4393.0551.....	4391.8213	44730.313	3	21967.111	4	1.7 ± 0.4	−1.47
4443.7949.....	4442.5477	32620.018	2	10116.729	3	0.90 ± 0.10	−1.88
4446.7902.....	4445.5422	32620.018	2	10131.887	1	0.090 ± 0.011	−2.87
4500.1870.....	4498.9249	40787.857	2	18566.558	1	0.050 ± 0.011	−3.12
4555.8740.....	4554.5973	40516.243	2	18566.558	1	0.108 ± 0.022	−2.78
4685.4066.....	4684.0956	36844.710	1	15501.845	2	0.102 ± 0.013	−3.00
4832.5644.....	4831.2145	42660.058	3	21967.111	4	0.047 ± 0.011	−2.94
5034.9379.....	5033.5342	36844.710	1	16983.492	0	0.160 ± 0.028	−2.74
5045.4576.....	5044.0510	35321.653	3	15501.845	2	0.095 ± 0.016	−2.60
5229.1008.....	5227.6454	32620.018	2	13496.271	2	0.41 ± 0.07	−2.07

NOTE.—Table 3 is also available in machine-readable form in the electronic edition of the *Astrophysical Journal.*

[a] Vacuum wavelengths are computed from energy levels.

[b] Air wavelengths are computed from the energy levels using the standard index of air (Edlén 1953, 1966).

[c] Energy levels are from Blaise et al. (1992a).

TABLE 4

Comparison of Branching Fractions for Pt I Arranged by Upper Level

λ in Vacuum[a] (Å)	λ in Air[b] (Å)	Upper Level[c] (cm^{-1})	Upper J	Lower Level[c] (cm^{-1})	Lower J	Branching Fraction	
						Lotrian & Guern[d]	This Experiment
3315.9958	3315.0417	30156.854	4	0.000	3	0.121	0.119 ± 0.004
3409.1092	3408.1314	30156.854	4	823.678	4	0.879	0.881 ± 0.004
3065.6022	3064.7114	32620.018	2	0.000	3	0.901	0.9260 ± 0.0021
3140.2966	3139.3870	32620.018	2	775.892	2	0.044	0.0487 ± 0.0009
4443.7949	4442.5477	32620.018	2	10116.729	3	0.017	0.0124 ± 0.0013
4446.7902	4445.5422	32620.018	2	10131.887	1	0.004	0.00125 ± 0.00013
5229.1008	5227.6454	32620.018	2	13496.271	2	0.010	0.0057 ± 0.0009
2930.6464	2929.7892	34122.165	3	0.000	3	0.318	0.377 ± 0.004
2998.8359	2997.9618	34122.165	3	775.892	2	0.496	0.560 ± 0.004
3003.1395	3002.2643	34122.165	3	823.678	4	0.139	0.0297 ± 0.0007
3629.1444	3628.1100	34122.165	3	6567.461	2	0.028	0.0179 ± 0.0011
4165.7231	4164.5491	34122.165	3	10116.729	3	0.0115	0.0104 ± 0.0010
2250.0041	2249.3068	44444.364	2	0.000	3	0.219	0.195 ± 0.010
2289.9817	2289.2757	44444.364	2	775.892	2	0.228	0.230 ± 0.008
2640.1314	2639.3449	44444.364	2	6567.461	2	0.207	0.221 ± 0.012
2913.1048	2912.2520	44444.364	2	10116.729	3	0.130	0.143 ± 0.013
2914.3918	2913.5386	44444.364	2	10131.887	1	0.167	0.144 ± 0.013
3231.2169	3230.2843	44444.364	2	13496.271	2	0.047	0.056 ± 0.007
3455.1243	3454.1347	44444.364	2	15501.845	2	...	0.0059 ± 0.0021
3864.3152	3863.2199	44444.364	2	18566.558	1	...	0.0047 ± 0.0009
2165.8905	2165.2109	46170.386	2	0.000	3	0.378	0.361 ± 0.007
2202.9103	2202.2230	46170.386	2	775.892	2	0.417	0.357 ± 0.006
2525.0660	2524.3068	46170.386	2	6567.461	2	0.155	0.180 ± 0.010
2773.6437	2772.8251	46170.386	2	10116.729	3	...	0.0170 ± 0.0029
2774.8103	2773.9914	46170.386	2	10131.887	1	0.049	0.038 ± 0.004
3060.5267	3059.6371	46170.386	2	13496.271	2	...	0.0190 ± 0.0027
3260.6703	3259.7303	46170.386	2	15501.845	2	...	0.021 ± 0.003
3622.6860	3621.6533	46170.386	2	18566.558	1	...	0.0047 ± 0.0010

[a] Vacuum wavelengths are computed from energy levels.
[b] Air wavelengths are computed from the energy levels using the standard index of air (Edlén 1953, 1966).
[c] Energy levels are from Blaise et al. (1992a).
[d] Lotrian & Guern (1982).

defined to sum to one. Relative intensities accurate to 20% can yield branching fractions for dominant lines that are more accurate than ±20%.

Reader et al. (1990) and Sansonetti et al. (1992) made no claims as to whether or not their source was optically thin. We knew from the type of lamp they used and from the operating conditions they used that some of the strong lines to low-lying levels were likely to need an optical depth correction. We initially planned to use our measurements made with a grating spectrometer to correct those few lines and then use intensities from the NIST Atlas for many other longer wavelength lines. This plan had to be abandoned when we discovered a large wavelength-dependent radiometric calibration error in the NIST Atlas. This problem was discussed with NIST personnel in mid-2003, and they subsequently confirmed that there is a calibration problem (C. J. Sansonetti 2003, private communication; G. Nave 2003, private communication).

Table 5 compares some of our new branching ratio measurements with branching ratios from the NIST Atlas. These comparisons were chosen so that the line ratios are not prone to errors from a nonnegligible optical depth. The ratios tend to agree for lines with a small wavenumber separation but disagree in a systematic fashion for lines with larger separations. The red lines from a given upper level in the NIST Atlas are too strong in comparison with blue lines from the same upper level. Errors in this direction can be caused by a nonnegligible optical depth, but there is a more serious radiometric calibration problem in the NIST Atlas. Our intent is not to belabor this point but simply to alert readers and *HST* users to the fact that the intensities of widely separated lines in the NIST Atlas are not reliable. Relative intensities of lines from the NIST Atlas with small separations are reliable. Wavelengths from the NIST Atlas should be unaffected by the intensity errors. New measurements on Pt intensities are underway at NIST using the NIST 2 m FTS (G. Nave 2003, private communication). Deep UV intensity measurements are technically difficult.

Independent branching fraction measurements often do not achieve the excellent agreement that is routine for independent LIF measurements of radiative lifetimes. Branching fraction measurements in the UV and vacuum UV (VUV) are especially challenging. The use of FTS instruments in the UV helps, but better (internal) radiometric calibration techniques are needed in the UV and VUV. Further improvement of FTS performance in the VUV is also needed.

4. PLATINUM IN METAL-POOR STARS AND THE SUN

Easily detectable Pt I lines in cool stellar spectra occur only in the ultraviolet, $\lambda < 3400$ Å. In their solar photospheric platinum abundance study, Youssef & Khalil (1987) affirm that this spectral region "is crowded by strongly perturbed lines of many elements and platinum may only be a minor contributor to the observed absorption feature, in addition to the uncertainty of the continuum location." Their warning applies to all five solar Pt I identifications in this wavelength domain in the spectral

TABLE 5
Comparison of Pt I Line Intensity Ratios Arranged by Upper Level

Upper Level[a] (cm^{-1})	λ (1) Vacuum[b] (Å)	λ (2) Vacuum[b] (Å)	Intensity(1)/Intensity(2)	
			NIST[c]	This Experiment
34122.165	3629.1444	3003.1395	1.4 ± 0.4	0.60 ± 0.04
34122.165	4165.7231	3003.1395	1.2 ± 0.4	0.35 ± 0.03
35321.653	3967.4787	2898.7209	1.7 ± 0.5	0.44 ± 0.04
36296.310	3819.7708	2819.0747	7.5 ± 2.1	1.95 ± 0.14
37342.101	3675.0905	3673.0444	0.78 ± 0.22	0.63 ± 0.07
37342.101	4193.6053	3673.0444	1.5 ± 0.4	0.79 ± 0.08
37769.073	4119.8375	3204.9626	0.74 ± 0.21	0.272 ± 0.019
38815.908	3484.4202	3100.9245	0.53 ± 0.15	0.275 ± 0.014
38815.908	3486.2616	3100.9245	2.7 ± 0.8	1.48 ± 0.04
38815.908	3949.5037	3100.9245	0.62 ± 0.17	0.155 ± 0.013
38815.908	4289.2567	3100.9245	0.21 ± 0.06	0.041 ± 0.004
40516.243	3291.1673	2945.6138	5.1 ± 1.4	4.0 ± 0.3
40516.243	3700.9661	2945.6138	3.0 ± 0.9	1.32 ± 0.15
40516.243	3997.6976	2945.6138	2.4 ± 0.7	0.58 ± 0.08
40787.857	3664.1330	2922.2339	1.2 ± 0.3	0.29 ± 0.04

[a] Energy levels are from Blaise et al. (1992a).
[b] Vacuum wavelengths are computed from energy levels.
[c] Sansonetti et al. (1992).

atlas of Moore et al. (1966). Therefore, following our procedure used previously in deriving a photospheric holmium abundance from similarly entangled near-UV Ho II features (Lawler et al. 2004), we first searched for detectable Pt I lines in the spectrum of a star that (1) is very metal-poor, (2) possesses very enhanced neutron capture (*n*-capture; $Z > 30$) elemental abundances, and (3) has an *n*-capture abundance distribution indicative of rapid bombardment (*r*-process) nucleosynthesis. The combination of a generally weak-lined spectrum and supersolar *r*-process abundance ratios in such a star can often reveal transitions of the heaviest *n*-capture elements (e.g., Os, Ir, Pt) that otherwise would be masked by strong Fe peak and molecular features.

4.1. *Platinum in BD +17°3248*

Detection of Pt I in metal-poor stars was first reported by Sneden et al. (1998). In their Figure 1, the 2929.79 and 3064.71 Å lines are clearly present in the *HST* GHRS spectrum of HD 115444 but undetectably weak in the spectrum of HD 122563. This contrast in Pt I strengths is reasonable, as HD 115444 and HD 122563 have similar metallicities ([Fe/H] = −2.91 and −2.74, respectively; Westin et al. 2000)[3] but sharply contrasting relative abundances of the heavier *r*-process elements (e.g., [Eu/Fe] = +0.85 and −0.36, respectively; Westin et al.). Later, Cowan et al. (2002) identified Pt I lines at 2646.88, 2650.85, 2659.45, 2929.79, and 3064.71 Å in their *HST* STIS spectra of BD +17°3248 ([Fe/H] = −2.09; [Eu/Fe] = +0.91), deriving a platinum abundance enhancement similar to that of europium: [Pt/Fe] = +0.96 or [Pt/Eu] = +0.05. Recently, Sneden et al. (2003) derived the abundances or meaningful upper limits for 57 elements including platinum in the well-studied halo giant CS 22892–052, a low-metallicity star ([Fe/H] = −3.12) with extreme *r*-process enhancements (e.g., [Eu/Fe] = +1.64). A large platinum overabundance was also found ([Pt/Fe] ≃ +1.6), but the S/N of the *HST* STIS spectrum of this faint star was low, S/N ≃ 20, allowing analysis of only a few Pt I lines, with a resulting large abundance uncertainty. In the end we chose BD +17°3248 for the present Pt I line identification exercise because the Cowan et al. (2002) spectra for this star have both high resolution ($R = \lambda/\Delta\lambda \geq 30000$) and S/N > 50 over the entire 2600–4000 Å spectral range occupied by strong Pt I transitions.

In LTE, relative absorption strengths among lines of a given species vary as $\log(gf) - 5040E_l/T$, where E_l is the lower excitation potential in eV. Using the effective temperature $T_{\rm eff} = 5200$ K of BD +17°3248 in this relationship, the relative strength measures of the five Pt I lines studied by Cowan et al. (2002) are all in the range −0.1 to −1.1. Inspection of four of these lines in Figure 5 of that paper suggests that a Pt I line would be undetectable in BD +17°3248 if its strength measure falls below ∼−3.0. We therefore neglected lines from Table 3 that were weaker than this limit.

The short-wavelength limit of the Cowan et al. (2002) BD +17°3248 *HST* STIS spectrum is 2300 Å. In addition, its S/N decreases toward that limit, and contamination from other species is large in the 2300–2600 Å range. We therefore further narrowed the useful list of lines by eliminating those with $\lambda < 2600$ Å. This left about 45 of the original set of 128 Pt I lines for potential detection in BD +17°3248. Of these, about 20 have $\lambda > 3000$ Å. Consultation of the Moore et al. (1966) solar line list and the Delbouille et al. (1973)[4] center-of-disk solar spectrum revealed some atomic and/or molecular blends so severe that the Pt I contributions would be masked in the spectra of the Sun and BD +17°3248. Inspection of the ultraviolet solar observed/synthetic spectral atlas of Kurucz & Avrett (1981) served to identify a few more obvious cases of severely blended Pt I lines. These lines were also eliminated from further consideration.

We treated in more detail the remaining ∼20 Pt I lines from the Table 3 original set. As in previous papers of this series (Lawler et al. 2004 and references therein), we used the Kurucz (1998)[5] line database to construct atomic and molecular hydride (predominantly OH, with some CH and/or NH) line lists

[3] For elements A and B, absolute abundances for the Sun or a star are defined as $\log \epsilon(\mathrm{A}) = \log_{10}(N_{\rm A}/N_{\rm H}) + 12.0$, and relative abundances between a star and the Sun are defined as $[\mathrm{A/B}] = \log_{10}(N_{\rm A}/N_{\rm H})_{\rm star} - \log_{10}(N_{\rm A}/N_{\rm H})_{\rm sun}$.

[4] Available at http://mesola.obspm.fr/solar_spect.php.

[5] Available at http://kurucz.harvard.edu/.

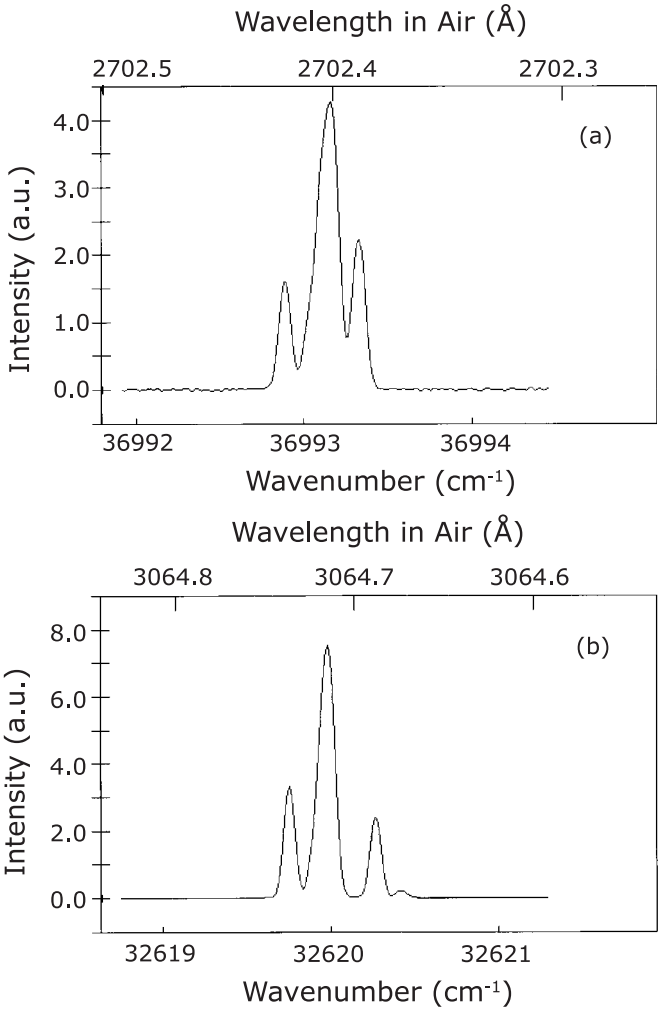

FIG. 3.—Profiles of selected Pt I lines from FTS data. Hyperfine structure of the odd isotope, ^{195}Pt, contributes the "outer" red- and blueshifted components. The strong central feature in the profiles is a blend of components from the even isotopes and from ^{195}Pt.

for 4–6 Å spectral intervals surrounding the Pt I transitions. For the Pt I lines we employed the log gf values from Table 3. Natural platinum has six isotopes: ^{190}Pt (0.014% of the elemental abundance in the solar system, from meteoritic data; e.g., Rosman & Taylor 1998;[6] Table 6 in Lodders 2003), ^{192}Pt (0.782%), ^{194}Pt (32.967%), ^{195}Pt (33.832%), ^{196}Pt (25.242%), and ^{198}Pt (7.163%). The transition wavelengths of these isotopes differ by 0.01–0.03 Å. In addition, the odd isotope ^{195}Pt exhibits hyperfine splitting of its energy levels, yielding 3–4 transition subcomponents separated by as much as 0.09 Å. Figure 3 shows some of the Pt I lines from FTS spectra. The isotopic and hyperfine splittings are large enough that Pt I transitions cannot be treated as single lines.

Not enough of the structure is resolved in the FTS data for a detailed analysis, but such an analysis is not necessary. A literature search revealed that many of the needed hyperfine and isotopic data are known. Hyperfine measurements on the two lowest lying even-parity levels, including the ground level and the level near 776 cm^{-1}, were made by Büttgenbach et al. (1984) using an extremely precise radiofrequency technique. Neu et al. (1987) made numerous hyperfine and isotope shift measurements on Pt I using a single-mode laser and an atomic beam apparatus. Hyperfine measurements on additional even- and odd-parity levels were made by Basar et al. (1996) using laser-optogalvanic spectroscopy in a hollow cathode lamp. Isotope shifts for numerous Pt I lines from laser-optogalvanic measurements, along with a table of residual level isotope shifts, were reported by Kronfeldt & Basar (1995). Residual level shifts are found by picking a reference (arbitrary) level to have zero isotope shift, subtracting the normal mass shift from transitions connected to that level, and then assigning the residual isotope shift to the other level involved in the transition. LaBelle et al. (1989) reported complete line structure patterns for two Pt I lines using Doppler-free saturation spectroscopy in a hollow cathode lamp with a single-mode laser. Some additional references to earlier work on Pt I line structures can be found in the five papers cited above, but these five contain the most useful recent results along with some weighted averages that include older measurements.

[6] Available at http://www.iupac.org/reports/1998/7001rosman/iso.pdf.

TABLE 6
PLATINUM ABUNDANCES IN BD +17°3248 FROM INDIVIDUAL Pt I FEATURES

λ IN AIR (Å)	EXCITATION POTENTIAL[a] (cm^{-1})	(eV)	log gf	log ϵ
2646.88	0.000	0.000	−0.786	0.62 ± 0.05
2650.85	823.678	0.102	−0.950	0.62 ± 0.10
2659.45	0.000	0.000	−0.025	0.42 ± 0.15
2702.40	775.892	0.096	−0.332	0.57 ± 0.15
2705.89	823.678	0.102	−0.489	0.52 ± 0.20
2771.66	775.892	0.096	−1.079	0.52 ± 0.15
2929.79	0.000	0.000	−0.696	0.52 ± 0.05
2997.96	775.892	0.096	−0.505	0.47 ± 0.20
3064.71	0.000	0.000	−0.325	0.47 ± 0.20
3315.04	0.000	0.000	−2.560	<0.5
3408.13	823.678	0.102	−1.670	0.4 ± 0.30

[a] Excitation potential or lower level energy.

The results of LaBelle et al. are in a convenient form for use by astronomers. Since the other line structure data are in less convenient forms, we have included our reconstructed, complete line structure patterns for the most important Pt I lines in the Appendix. These patterns give component positions relative to the center of gravity for the lines, and component strengths normalized so that they sum to unity.

We adopted the solar system isotopic abundance fractions in the stellar and solar computations. The LTE line analysis code MOOG (Sneden 1973) was employed to compute initial synthetic spectra of BD +17°3248 with these line lists. We adopted the model stellar atmosphere derived by Cowan et al. (2002): an ATLAS model interpolated from the Kurucz (1998) grid with parameters $T_{\rm eff} = 5200$ K, $\log g = 1.80$, $[{\rm M/H}] = -2.0$, and $v_{\rm micro} = 1.9$ km s^{-1}. The synthetic spectra were convolved with Gaussian functions of FWHM ≈ 0.12 Å to account for the combined effects of stellar macroturbulence and the spectrograph resolving power. Then these spectra were visually compared with the ground-based or *HST* observed spectra of Cowan et al. The immediate result of this work was to identify further cases of Pt I lines that are too blended to be of further use. In the end 11 Pt I lines were retained for abundance analysis in BD +17°3248; these are listed in Table 6. The line strengths of the atomic contaminants were varied to provide the best matches to the observed stellar (and solar redward of 3000 Å) spectra. The strengths of the OH, CH, or NH lines were altered in concert by varying the O, C, or N abundances.

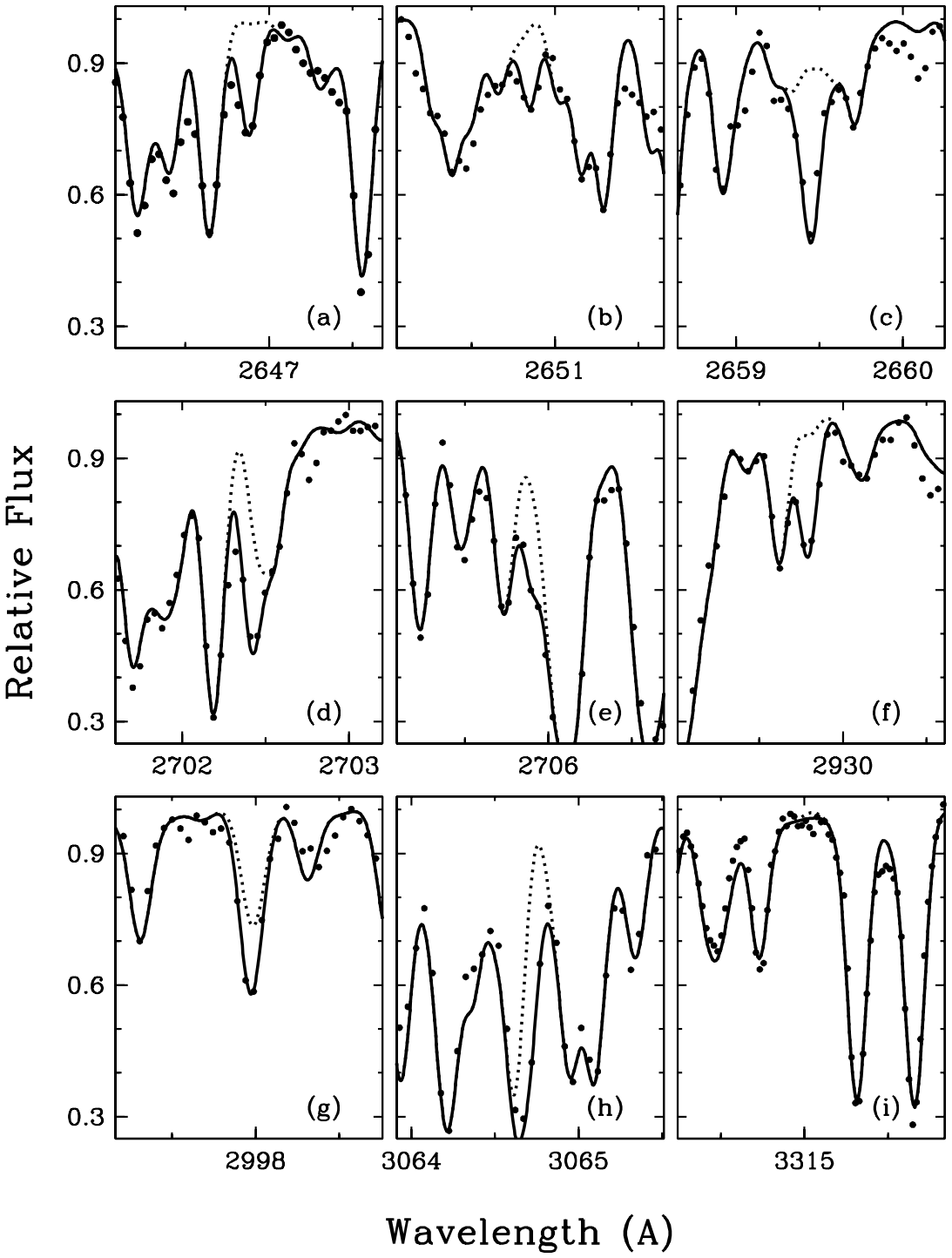

FIG. 4.—Observed and synthetic spectra of nine of the 11 Pt I features used in determining the platinum abundance of BD +17°3248. Only the 2771.66 and 3408.13 Å lines are not shown here. In each panel the observed spectrum (*filled circles*), the best-matching synthetic spectrum (*solid line*), and a synthetic spectrum with no Pt I contribution (*dotted line*) are shown.

No changes were made to the lab data for the Pt I lines. Platinum is overwhelmingly synthesized through the *r*-process. In solar system material the *r*-process elemental fraction is approximately 95% (Simmerer et al. 2005). We have therefore assumed a solar system isotopic mixture for Pt in this paper.

Repeated synthetic spectrum matches to the observed spectra yielded best-fit platinum abundances given in Table 6. The uncertainties entered for these values represent only "fit" uncertainties due to sources such as continuum placement, Pt I profile matching, and contamination by other species. In Figure 4 we show synthetic/observed spectrum matches for nine of the Pt I lines in BD +17°3248. In each panel two synthetic spectra are displayed, one computed without inclusion of Pt I and the other representing the best-fit synthesis. Inspection of these suggests that the 2647, 2660, and 2929 Å lines are mostly unblended in very metal-poor stellar spectra of BD +17°3248. The utility of these lines is dependent on the $T_{\rm eff}/\log g$ domain. The 2650 Å feature is blended but dominated by Pt I absorption; it is a useful secondary abundance indicator. The 2702, 2705, 2998, and 3064 Å (and 2771 Å, not shown in Fig. 4) lines are heavily

blended by other atomic and molecular transitions but can be employed as platinum abundance indicators. The reader is cautioned that any combination of overall metallicity [Fe/H] increase, [Pt/Fe] decrease, and $T_{\rm eff}$ decrease will cause all Pt I features to suffer more blending and thus increase the platinum abundance uncertainty. Finally, the 3315 and 3408 Å lines are so weak and/or blended that in all but the most platinum-rich stars they are best viewed as platinum abundance limit estimators.

A straight mean of the abundances in Table 6, neglecting the 3315 and 3408 Å lines, is $\langle \log \epsilon({\rm Pt}) \rangle = +0.53 \pm 0.02$ ($\sigma = 0.07$). The line-to-line scatter σ-value is consistent with the spectral feature matching uncertainties. Cowan et al. (2002) derived $\langle \log \epsilon({\rm Pt}) \rangle = +0.67$ ($\sigma = 0.05$) from five Pt I lines. The 0.14 dex abundance decrease in the present value is primarily due to the improvement in the characterization of the Pt I lines from the more reliable transition probabilities and the inclusion of isotopic and hyperfine splitting. For the BD +17°3248 Pt I spectrum the transition probability and transition substructure corrections are of comparable importance to the derived abundances. The influence of substructure will of course vary with overall Pt I line strengths in other stars.

Model atmosphere uncertainties have some influence in derived platinum abundances, particularly in comparisons of platinum with lighter *n*-capture elements. For typical Pt I, Fe I, and Fe II lines near 3000 Å and the well-studied Eu II line at 4129.8 Å, we computed abundance offsets in response to model parameter changes representative of the uncertainties derived by Cowan et al. (2002) for BD +17°3248. For a temperature change $\Delta T_{\rm eff} = \pm 150$ K, we derive $\Delta[{\rm Fe\ I/H}] = \pm 0.15$, $\Delta[{\rm Fe\ II/H}] = \pm 0.00$, $\Delta[{\rm Eu\ II/H}] = \pm 0.10$, and $\Delta[{\rm Pt\ I/H}] = \pm 0.20$. Therefore, this $T_{\rm eff}$ change results in $\Delta[{\rm Pt\ I/Eu\ II}] = \pm 0.10$. For a gravity change $\Delta \log g = \pm 0.3$, $\Delta[{\rm Fe\ I/H}] = \mp 0.14$, $\Delta[{\rm Fe\ II/H}] = \pm 0.02$, $\Delta[{\rm Eu\ II/H}] = \pm 0.07$, and $\Delta[{\rm Pt\ I/H}] = \pm 0.00$. Therefore, this $\log g$ change results in $\Delta[{\rm Pt\ I/Eu\ II}] = \pm 0.07$. Varying the assumed model metallicity in the range $\Delta[{\rm M/H}] = \pm 0.20$ induced no substantial variations in any of the derived abundances. Finally, microturbulent velocity variations $\Delta v_{\rm micro} = \pm 0.2$ km s^{-1} yielded abundance variations from 0.0 to 0.1, depending on the strengths of the lines in question. Model atmosphere parameters for BD +17°3248 were determined by Cowan et al. from a combination of broadband photometry and excitation/ionization balances of Fe peak spectral features. Thus, the $T_{\rm eff}$ and $\log g$ parameters are not independent; e.g., an increase in $T_{\rm eff}$ would increase the ion-to-neutral ratio, which would in turn necessitate an increase in $\log g$ to compensate. These correlated variations suggest that Δ[Pt/Eu] can be as much as 0.15–0.20 with large changes in $T_{\rm eff}$ and $\log g$. This caution should be kept in mind in interpreting *n*-capture abundance distributions that include the rare earths (always detected in the first ionized species) and the heaviest stable elements (e.g., Os, Ir, Pt, Au, Pb, always detected in the neutral species).

Cowan et al. (2002) studied nearly 30 *n*-capture elements in BD +17°3248; see that paper for an extended discussion of the major abundance trends in the *n*-capture domain. Here we limit our comments to a comparison of the new platinum abundance with europium. Cowan et al. derived $\langle \log \epsilon({\rm Eu}) \rangle = -0.67 \pm 0.02$ ($\sigma = 0.05$), yielding $\log \epsilon({\rm Pt/Eu}) = +1.20$. Simmerer et al. (2005) have computed the most recent breakdown of solar system elemental abundances into *r*- and *s*-process components. Since BD +17°3248 is an *r*-process–rich star, the proper comparison is with the solar system *r*-only abundances (col. [5] of Table 10 of Simmerer et al.): $\log \epsilon({\rm Pt/Eu})_{\rm SS} = +1.654 - 0.494 = +1.160$. The BD +17°3248 and solar system *r*-process Pt/Eu abundance ratios are thus now in excellent agreement.

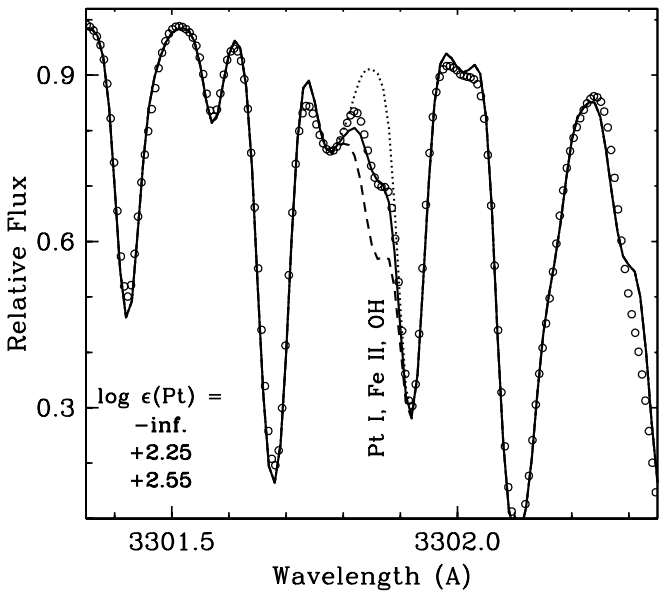

FIG. 5.—Observed and synthetic spectra of the 3301.86 Å Pt I line in the solar photosphere. The open circles represent the observed spectrum (Delbouille et al. 1973). Their spectrum has a wavelength interval of 0.002 Å between points in this wavelength region, but for display purposes in this figure we only have plotted every third point (i.e., a step size of 0.006 Å). The assumed platinum abundances of the synthetic spectra are indicated in the figure, and we emphasize that the dotted-line spectrum [$\log \epsilon({\rm Pt}) = -4$] has been computed with the Pt I feature removed entirely.

4.2. *Platinum in the Solar Photosphere*

The most recent solar system abundance compilation by Lodders (2003) adopts $\log \epsilon({\rm Pt}) = 1.67 \pm 0.03$ for the platinum meteoritic abundance and 1.74 for the solar photospheric value. These numbers are in basic agreement with previous recommendations by Grevesse and collaborators (Grevesse & Sauval 1998 and references therein). However, the photospheric abundance comes from the pioneering analysis by Youssef & Khalil (1987) of just a single Pt I line at 3301.86 Å. Therefore, Lodders does not even attach a formal uncertainty to this value. We did not recommend the 3301 Å line as a platinum abundance indicator for BD +17°3248. Here we suggest that this line is a very blended feature and probably should be discarded as a photospheric platinum abundance indicator.

In Figure 5 we show a small spectral interval surrounding the 3301.86 Å Pt I line. The observed spectrum is that of Delbouille et al. (1973). This figure is very similar to Figure 1 of Youssef & Khalil (1987), who identify many of the other species that are competing with Pt I absorption. The synthetic/observed spectrum match in Figure 5 is obviously very good, but the reader should remember that the agreement is forced for lines away from the Pt I location. In particular, we adjusted the transition probabilities of the Ti II line at 3301.67 Å and the very strong Fe I line at 3301.92 Å to better match the photospheric spectrum; these lines directly affect the derived platinum abundance. However, the major problems here are lines of Fe II and OH, two contaminants that appear in the Kurucz (1998) line lists at essentially the same wavelength as that of the Pt I line. The synthetic spectra of Figure 5 have been generated with no alteration to the Kurucz transition probabilities of the Fe II and OH lines. With this choice, the best-fit synthesis to the observed solar feature yields $\log \epsilon({\rm Pt}) \approx +2.25$, a factor of 3 larger than the meteoritic value. If the contribution of the Fe II and OH lines were to be decreased, the implied platinum

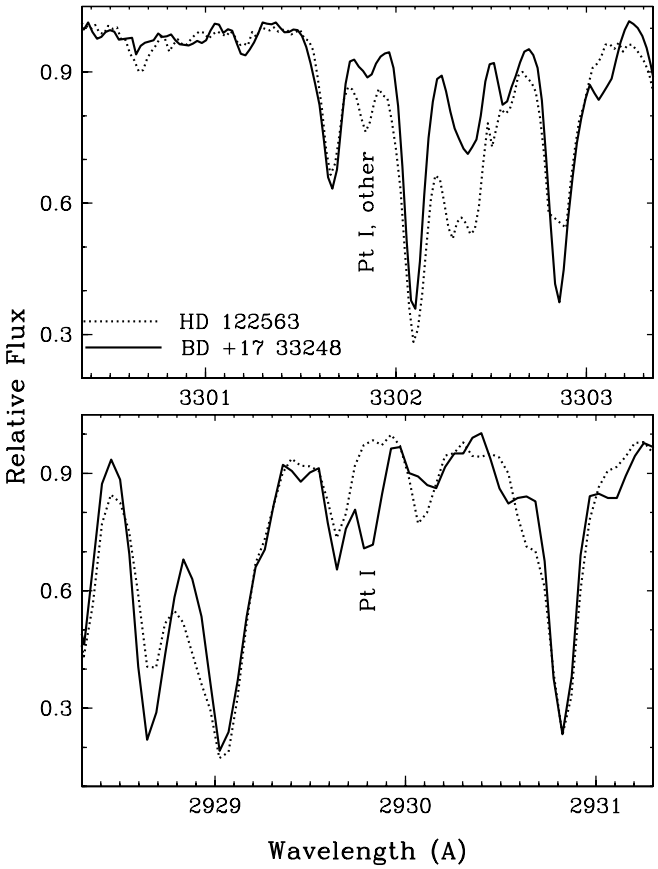

FIG. 6.—Comparison of two small spectrum regions in the high-resolution spectra of BD +17°3248 (*r*-process–rich) and HD 122563 (*r*-process–poor). In (*a*) the alleged Pt I line at 3301.86 Å is labeled. In (*b*) the nearly unblended 2929.79 Å line is labeled; the BD +17°3248 spectrum in this panel is the same one displayed as filled circles in Fig. 2*f*.

abundance would become even larger. We can force the solar abundance to agree with the meteoritic abundance by large increases in the Fe II and/or OH transition probabilities, but we know of no laboratory studies to justify this action.

Additional concerns about the Pt I 3301 Å line can be found by reconsideration of BD +17°3248. In Figure 6 we compare the spectra of this *r*-process–rich low-metallicity star with the *r*-process–poor star HD 122563 (Westin et al. 2000) in the spectral regions immediately surrounding the 3301.86 and 2929.79 Å lines. Figure 6*b* is very similar to Figure 1 of Sneden et al. (1998) and makes the same point: the 2929 Å line tracks the platinum abundance very well in low-metallicity giants and correlates almost equally well with lighter *r*-process indicators such as europium. The spectra of Figure 6*a* tell a different story: the absorption at 3301.86 Å is much stronger in HD 122563 than it is in BD +17°3248. Repeated trial spectrum syntheses indicate that some combination of Fe II, OH, and probably some other low-temperature absorber (perhaps NH, which is present in this spectral region) is largely responsible for the absorption seen here.

Consideration of the spectra of the solar photosphere and two metal-poor stars with contrasting Pt I absorption strengths strongly suggests that the 3301.86 Å Pt I line is not a useful feature in platinum abundance studies. Unfortunately, our hunt for other potentially useful Pt I lines in the solar spectrum yielded nothing; all other strong Pt I lines appear to be hopelessly blended with other atomic and/or molecular contaminants. Discarding the 3301 Å line thus leaves no other promising photospheric Pt I feature for analysis. We have little choice here but to recommend that the solar system platinum abundance be taken exclusively from the meteoritic value, and the nominal photospheric value be neglected in future solar abundance compendiums.

5. SUMMARY

Radiative lifetimes for 58 odd-parity levels of Pt I were measured using time-resolved LIF on a slow beam of Pt atoms. Branching fractions for 127 lines of Pt I were measured using a grating spectrometer and an FTS. The new Pt lifetime measurements were found to be in good agreement with earlier LIF measurements. The new branching fraction measurements were found to be in fair agreement with one earlier study. The new lifetimes and branching fractions were combined to yield improved atomic transition probabilities for lines of Pt I. These laboratory results were applied to determine the abundance of Pt in the metal-poor Galactic halo star BD +17°3248. An attempt to refine the solar photospheric abundance of Pt was unsuccessful. The blending of the 3301 Å line, the only Pt I line used in earlier solar abundance studies, was found to be more severe than expected from these earlier studies.

Laboratory measurements reported herein were supported by National Science Foundation grant AST 02-05124 (J. E. L. and E. D. H.). Astrophysical applications reported herein were supported by National Science Foundations grants AST 99-87162 (C. S.), AST 03-07495 (C. S.), AST 99-86974 (J. J. C.), and AST 03-07279 (J. J. C.), PHY 02-16783: Physics Frontiers Center/JINA: Joint Institute for Nuclear Astrophysics (T. C. B.), and by STScI under grant GO-08342 (J. J. C., T. C. B., and C. S.). J. E. Lawler is a guest observer at the National Solar Observatory, and he is indebted to Mike Dulick and Detrick Branstron for help in accessing archived spectra. The NSO FTS spectra of Pt were recorded by R. Engleman Jr., L. M. Faires, J. W. Brault, R. P. Hubbard, and J. G. Lyon. We acknowledge their contributions. Part of this work was completed while C. S. was a visiting scientist at Carnegie Observatories; their hospitality and financial support are greatly appreciated.

APPENDIX A

Hyperfine and isotopic structure of Pt I lines should not be neglected in the abundance determinations. Complete (reconstructed) line structure patterns for selected Pt I lines are given in Table 7 for the user's convenience. Wavenumbers of transitions were computed from the energy levels (Blaise et al. 1992a), and the air wavelengths were computed from the energy levels using the standard index of air (Edlén 1953, 1966). Isotopic abundances for Pt were taken from Rosman & Taylor (1998). Components with half-integral *F* values, the first three or four components of each transition, are all from ^{195}Pt. The component strengths from ^{195}Pt

TABLE 7

COMPLETE LINE STRUCTURE PATTERNS FOR SELECTED Pt I LINES

Transition Wavenumber (cm^{-1})	λ in Air (Å)	Upper F	Lower F	Relative Component Position[a] (cm^{-1})	Relative Component Position[a] (Å)	Normalized Component Strength[b]	References[c]
37769.073.....	2646.8807	3.5	3.5	−0.1859	0.01303	0.18642	1, 2, 3
			2.5	0.4799	−0.03363	0.00690	1, 2, 3
		2.5	3.5	−0.4097	0.02871	0.00690	1, 2, 3
			2.5	0.2561	−0.01795	0.13809	1, 2, 3
		3	3	0.0948	−0.00665	0.00014	1, 2, 3
				0.0604	−0.00423	0.00782	1, 2, 3
				0.0218	−0.00153	0.32967	1, 2, 3
				−0.0178	0.00125	0.25242	1, 2, 3
				−0.0608	0.00426	0.07163	1, 2, 3
37590.569.....	2659.4505	4.5	3.5	−0.1894	0.01340	0.18796	1, 2, 3
		3.5	3.5	−0.3951	0.02795	0.00537	1, 2, 3
			2.5	0.2707	−0.01915	0.14499	1, 2, 3
		4	3	0.1204	−0.00852	0.00014	1, 2, 3
				0.0766	−0.00542	0.00782	1, 2, 3
				0.0276	−0.00196	0.32967	1, 2, 3
				−0.0226	0.00160	0.25242	1, 2, 3
				−0.0772	0.00546	0.07163	1, 2, 3
36993.181.....	2702.3993	3.5	2.5	0.1890	−0.01381	0.19333	4, 4, 4
		2.5	2.5	−0.0348	0.00254	0.00967	4, 4, 4
			1.5	−0.2522	0.01842	0.13533	4, 4, 4
		3	2	0.1651	−0.01206	0.00014	4, 4, 4
				0.1048	−0.00766	0.00782	4, 4, 4
				0.0379	−0.00277	0.32967	4, 4, 4
				−0.0311	0.00227	0.25242	4, 4, 4
				−0.1059	0.00774	0.07163	4, 4, 4
36945.395.....	2705.8949	3.5	4.5	0.0535	−0.00392	0.18796	4, 4, 4
			3.5	0.1809	−0.01325	0.00537	4, 4, 4
		2.5	3.5	−0.0429	0.00314	0.14499	4, 4, 4
		3	4	0.3729	−0.02731	0.00014	4, 4, 4
				0.2366	−0.01733	0.00782	4, 4, 4
				0.0855	−0.00626	0.32967	4, 4, 4
				−0.0703	0.00515	0.25242	4, 4, 4
				−0.2394	0.01754	0.07163	4, 4, 4
36068.818.....	2771.6595	1.5	2.5	0.0623	−0.00479	0.20299	1, 2, 3
			1.5	−0.1553	0.01194	0.02255	1, 2, 3
		0.5	1.5	−0.0728	0.00560	0.11277	1, 2, 3
		1	2	0.0740	−0.00569	0.00014	1, 2, 3
				0.0471	−0.00362	0.00782	1, 2, 3
				0.0170	−0.00131	0.32967	1, 2, 3
				−0.0139	0.00107	0.25242	1, 2, 3
				−0.0475	0.00365	0.07163	1, 2, 3
34122.165.....	2929.7892	3.5	3.5	−0.1292	0.01109	0.18642	1, 2, 3
			2.5	0.5366	−0.04607	0.00690	1, 2, 3
		2.5	3.5	−0.4881	0.04191	0.00690	1, 2, 3
			2.5	0.1777	−0.01526	0.13809	1, 2, 3
		3	3	0.0623	−0.00535	0.00014	1, 2, 3
				0.0397	−0.00341	0.00782	1, 2, 3
				0.0143	−0.00123	0.32967	1, 2, 3
				−0.0117	0.00101	0.25242	1, 2, 3
				−0.0400	0.00343	0.07163	1, 2, 3
33346.273.....	2997.9618	3.5	2.5	0.2459	−0.02211	0.19333	1, 2, 3
		2.5	2.5	−0.1130	0.01016	0.00967	1, 2, 3
			1.5	−0.3306	0.02973	0.13533	1, 2, 3
		3	2	0.1348	−0.01211	0.00014	1, 2, 3
				0.0858	−0.00771	0.00782	1, 2, 3
				0.0309	−0.00278	0.32967	1, 2, 3
				−0.0253	0.00228	0.25242	1, 2, 3
				−0.0864	0.00777	0.07163	1, 2, 3

TABLE 7—*Continued*

Transition Wavenumber (cm^{-1})	λ in Air (Å)	Upper F	Lower F	Relative Component Position[a] (cm^{-1})	Relative Component Position[a] (Å)	Normalized Component Strength[b]	References[c]
32620.018.....	3064.7114	2.5	3.5	−0.2198	0.02065	0.19333	1, 2, 3
		2.5	2.5	0.4460	−0.04191	0.00967	1, 2, 3
		1.5	2.5	0.2918	−0.02742	0.13533	1, 2, 3
		2	3	0.1048	−0.00984	0.00014	1, 2, 3
				0.0667	−0.00626	0.00782	1, 2, 3
				0.0241	−0.00226	0.32967	1, 2, 3
				−0.0197	0.00185	0.25242	1, 2, 3
				−0.0672	0.00631	0.07163	1, 2, 3
30277.249.....	3301.8593	1.5	2.5	−0.0914	0.00997	0.20299	1, 5, 3
		1.5	1.5	0.0826	−0.00901	0.02255	1, 5, 3
		0.5	1.5	0.1651	−0.01801	0.11277	1, 5, 3
		1	2	0.1533	−0.01672	0.00014	1, 5, 3
				0.0976	−0.01064	0.00782	1, 5, 3
				0.0352	−0.00384	0.32967	1, 5, 3
				−0.0288	0.00314	0.25242	1, 5, 3
				−0.0984	0.01073	0.07163	1, 5, 3

NOTE.—Table 7 is also available in machine-readable form in the electronic edition of the *Astrophysical Journal.*

[a] Component position relative to the center of gravity of the transition as given in the first two columns. The center-of-gravity wavenumbers and wavelengths in the first two columns are for a solar isotopic mix.

[b] Component strengths normalized so that they sum to unity.

[c] The first reference gives the source of the isotope shifts, the second reference gives the source of the lower level hyperfine constant, and the third reference gives the source of the upper level hyperfine constant.

REFERENCES.—(1) Kronfeldt & Basar 1995; (2) Büttgenbach et al. 1984; (3) Basar et al. 1996; (4) LaBelle et al. 1989; (5) Neu et al. 1987.

always sum to 0.33832 (within rounding error). The first component with integral F for each transition, which always has component strength 0.00014, is ^{190}Pt. The other even isotopes, ^{192}Pt (0.00782), ^{194}Pt (0.32967), ^{196}Pt (0.25242), and ^{198}Pt (0.07163), are listed following ^{190}Pt. Relative component strengths would need to be modified to model nonsolar isotopic abundances. The center-of-gravity wavenumbers and wavelengths for a solar isotopic abundance in Table 7 would also need to be slightly modified for a nonsolar isotopic abundance.

REFERENCES

Adams, D. L., & Whaling, W. 1981, J. Opt. Soc. Am., 71, 1036
Anderson, H. M., Den Hartog, E. A., & Lawler, J. E. 1996, J. Opt. Soc. Am. B, 13, 2382
Basar, G., Kronfeldt, H.-D., & Kröger, S. 1996, Z. Phys. D, 36, 35
Biémont, E., Baudoux, M., Kurucz, R. L., Ansbacher, W., & Pinnington, E. H. 1991, A&A, 249, 539
Biémont, E., Palmeri, P., Quinet, P., Zhang, Z. G., & Svanberg, S. 2002, ApJ, 567, 1276
Blackwell, D. E., Ibbetson, P. A., Petford, A. D., & Shallis, M. J. 1979a, MNRAS, 186, 633
Blackwell, D. E., Petford, A. D., & Shallis, M. J. 1979b, MNRAS, 186, 657
Blaise, J., Vergès, J., Wyart, J.-F., & Engleman, R., Jr. 1992a, J. de Phys. II, 2, 947
———. 1992b, J. Res. NIST, 97, 213
Bord, D. J., Cowley, C. R., & Mirijanian, D. 1998, Sol. Phys., 178, 221
Brault, J. W. 1976, J. Opt. Soc. Am., 66, 1081
Bridges, J. M., & Ott, W. R. 1977, Appl. Opt., 16, 367
Büttgenbach, S., Glaeser, N., Roski, B., & Träber, F. 1984, Z. Phys. A, 317, 237
Cowan, J. J., Burris, D. L., Sneden, C., McWilliam, A., & Preston, G. W. 1995, ApJ, 439, L51
Cowan, J. J., Sneden, C., Truran, J. W., & Burris, D. L. 1996, ApJ, 460, L115
Cowan, J. J., et al. 2002, ApJ, 572, 861
Curry, J. J., Den Hartog, E. A., & Lawler, J. E. 1997, J. Opt. Soc. Am. B, 14, 2788
Danzmann, K., & Kock, M. 1982, J. Opt. Soc. Am., 72, 1556
Delbouille, L., Roland, G., & Neven, L. 1973, Photometric Atlas of the Solar Spectrum from λ3000 to λ10000 (Liège: Inst. Ap. Univ. Liège)
Den Hartog, E. A., Curry, J. J., Wickliffe, M. E., & Lawler, J. E. 1998, Sol. Phys., 178, 239
Den Hartog, E. A., Fedchak, J. A., & Lawler, J. E. 2001, J. Opt. Soc. Am. B, 18, 861
Den Hartog, E. A., Lawler, J. E., Sneden, C., & Cowan, J. J. 2003, ApJS, 148, 543
Den Hartog, E. A., Wickliffe, M. E., & Lawler, J. E. 2002, ApJS, 141, 255
Den Hartog, E. A., Wiese, L. M., & Lawler, J. E. 1999, J. Opt. Soc. Am. B, 16, 2278
Edlén, B. 1953, J. Opt. Soc. Am., 43, 339
———. 1966, Metrologia, 2, 71
Fedchak, J. A., Den Hartog, E. A., Lawler, J. E., Palmeri, P., Quinet, P., & Biémont, E. 2000, ApJ, 542, 1109
Gough, D. S., Hannaford, P., & Lowe, R. M. 1982, J. Phys. B, 15, L431
Gratton, R., & Sneden, C. 1994, A&A, 287, 927
Grevesse, N., & Sauval, A. J. 1998, Space Sci. Rev., 85, 161
Guo, B., Ansbacher, W., Pinnington, E. H., Ji, Q., & Berends, R. W. 1992, Phys. Rev. A, 46, 641
Hashiguchi, S., & Hasikuni, M. 1985, J. Phys. Soc. Japan, 54, 1290
Ivarsson, S., Litzén, U., & Wahlgren, G. M. 2001, Phys. Scr., 64, 455
Ivarsson, S., et al. 2003, A&A, 409, 1141
Klose, J. Z., Bridges, J. M., & Ott, W. R. 1988, J. Res. NBS, 93, 21
Kono, A., & Hattori, S. 1984, Phys. Rev. A, 29, 2981
Kronfeldt, H.-D., & Basar, G. 1995, Phys. Scr., 51, 227
Kurucz, R. L. 1998, in IAU Symp. 189, Fundamental Stellar Properties: The Interaction between Observation and Theory, ed. T. R. Bedding, A. J. Booth, & J. Davis (Dordrecht: Kluwer), 217
Kurucz, R. L., & Avrett, E. H. 1981, Solar Spectrum Synthesis. I. A Sample Altas from 224 to 300 nm (Cambridge: SAO)
LaBelle, R. D., Fairbank, W. M., Jr., Engleman, R., & Keller, R. A. 1989, J. Opt. Soc. Am. B, 6, 137
Lawler, J. E., Bonvallet, G., & Sneden, C. 2001a, ApJ, 556, 452
Lawler, J. E., Sneden, C., & Cowan, J. J. 2004, ApJ, 604, 850
Lawler, J. E., Wickliffe, M. E., Cowley, C. R., & Sneden, C. 2001b, ApJS, 137, 341
Lawler, J. E., Wickliffe, M. E., Den Hartog, E. A., & Sneden, C. 2001c, ApJ, 563, 1075
Lodders, K. 2003, ApJ, 591, 1220
Lotrian, J., & Guern, Y. 1982, J. Phys. B, 15, 1982
Lundberg, H., Johansson, S., Nilsson, H., & Zhang, Z. 2001, A&A, 372, L50

McWilliam, A., Preston, G. W., Sneden, C., & Searle, L. 1995, AJ, 109, 2757
Moore, C. E., Minnaert, M. G. J., & Houtgast, J. 1966, The Solar Spectrum 2935 Å to 8770 Å (NBS Monogr. 61; Washington, DC: NBS)
Neu, W., Passler, G., Sawatzky, G., Winkler, R., & Kluge, H.-J. 1987, Z. Phys. D, 7, 193
Nilsson, H., Ivarsson, S., Johansson, S., & Lundberg, H. 2002a, A&A, 381, 1090
Nilsson, H., Zhang, Z. G., Lundberg, H., Johansson, S., & Nordstrom, B. 2002b, A&A, 382, 368
Palmeri, P., Quinet, P., Wyart, J.-F., & Biémont, E. 2000, Phys. Scr., 61, 323
Quinet, P., Palmeri, P., Biemont, E., McCurdy, M. M., Rieger, G., Pinnington, E. H., Wickliffe, M. E., & Lawler, J. E. 1999, MNRAS, 307, 934
Ramanujam, P. S., & Andersen, T. 1978, ApJ, 226, 1171
Reader, J., Acquista, N., Sansonetti, C. J., & Sansonetti, J. E. 1990, ApJS, 72, 831
Rosman, K. J. R., & Taylor, P. D. P. 1998, J. Phys. Chem. Ref. Data, 27, 1275
Ryan, S. G., Norris, J. E., & Beers, T. C. 1996, ApJ, 471, 254
Sansonetti, J. E., Reader, J., Sansonetti, C. J., & Acquista, N. 1992, J. Res. NIST, 97, 1
Simmerer, J. A., Sneden, C., Cowan, J. J., Collier, J., Woolf, V. M., & Lawler, J. E. 2005, ApJ, in press
Sneden, C. 1973, ApJ, 184, 839
Sneden, C., Cowan, J. J., Burris, D. L., & Truran, J. W. 1998, ApJ, 496, 235
Sneden, C., McWilliam, A., Preston, G. W., Cowan, J. J., Burris, D. L., & Armosky, B. J. 1996, ApJ, 467, 819
Sneden, C., et al. 2003, ApJ, 591, 936
Volz, U., & Schmoranzer, H. 1998, in AIP Conf. Proc. 434, Atomic and Molecular Data and Their Applications, ed. P. J. Mohr & W. L. Wiese (Woodbury: AIP), 67
Weiss, A. W. 1995, Phys. Rev. A, 51, 1067
Westin, J., Sneden, C., Gustafsson, B., & Cowan, J. J. 2000, ApJ, 530, 783
Whaling, W., Carle, M. T., & Pitt, M. L. 1993, J. Quant. Spectrosc. Radiat. Transfer, 50, 7
Wickliffe, M. E., & Lawler, J. E. 1997, J. Opt. Soc. Am. B, 14, 737
Wickliffe, M. E., Lawler, J. E., & Nave, G. 2000, J. Quant. Spectrosc. Radiat. Transfer, 66, 363
Xu, H. L., Svanberg, S., Quinet, P., Garnir, H. P., & Biémont, E. 2003, J. Phys. B, 36, 4773
Yan, Z.-C., Tambasco, M., & Drake, G. W. F. 1998, Phys. Rev. A, 57, 1652
Youssef, N. H., & Khalil, N. M. 1987, A&A, 186, 333